Thesis Biobased Chemistry and Technology

Productivity of microalgal biomass constituents in simulated day night cycles

A model based approach

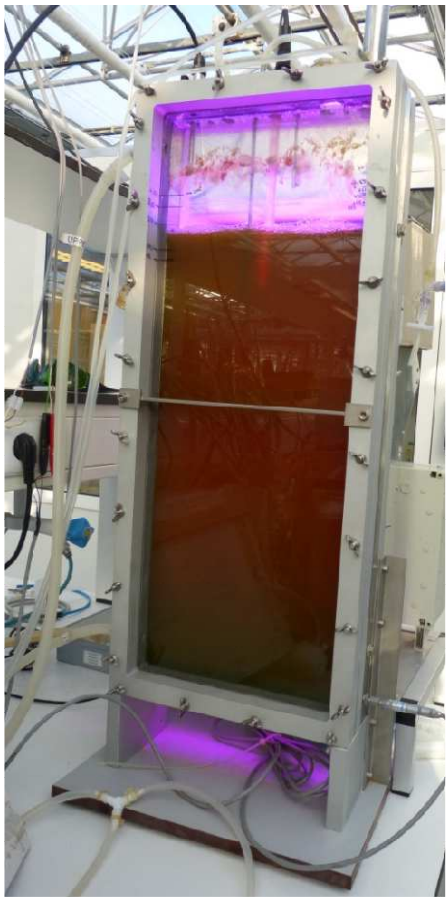

Kira Wieneke

March 17th, 2015

WAGENINGEN UNIVERSITY
AGROTECHNOLOGY AND
FOOD SCIENCES

Productivity of microalgal biomass constituents in simulated day night cycles

A model based approach

Name course:	Thesis project Biobased Chemistry and Technology
Number:	BCT-80436
Study load:	36 ECTS
Date:	March 17th, 2015

Student:	Kira Wieneke
Registration number:	900514-951-050
Study program:	MBT (Biotechnology)
Report number:	012BCT

Supervisors:	Ellen Puylaert-Slegers, Iago Dominguez Teles, Packo Lamers
Examiner:	Ton van Boxtel
Group:	Biobased Chemistry and Technology
Address:	Bornse Weilanden 9 6708 WG Wageningen, the Netherlands Tel: +31 (317) 48 21 24 Fax: +31 (317) 48 49 57

WAGENINGEN UNIVERSITY
AGROTECHNOLOGY AND
FOOD SCIENCES

Declaration of originality

I hereby certify that I am the sole authors of this MSc thesis including the delivered data set and graphics that are used, unless no reference is denoted.

I certify that, to the best of my knowledge, this report does not infringe upon anyone's copyright nor violate any proprietary rights and that any ideas, techniques, quotations, or any other material from the achievements of other people included in this report are fully acknowledged in accordance with the standard referencing practices.

I declare that this is a true copy of my thesis, including any final revisions.

Wageningen, March 17th, 2015

Table of contents

1 Abstract

The imminent shortage of fuels can be overcome by producing oil for biofuel synthesis as the main product of microalgae cultivations. Improvements are required to turn biofuel production from microalgae profitable and modeling can be used as a tool to identify the bottlenecks. Models of microalgae cultivations need to describe accurately the biomass composition and concentration to define the commercial feedstock. Recently, a model predicting the productivities of biomass, starch and triacylglycerides under nitrogen depletion has been developed. This model includes both carbon partitioning and photosynthetic efficiency dependent on the extent of nitrogen depletion under continuous light. The model was previously validated for *Scenedesmus obliquus*. In this study, the applicability of the model to *Chlorococcum littorale* was confirmed for continuous light conditions after strain specific parameters were experimentally derived. Model predictions for outdoors are required, since commercial production of microalgae use sunlight. The first step of adjusting the model to outdoor conditions was taken by incorporating light changes and dark respiration based on experimental data. The total biomass yield on photons was similar in continuous light and day night cycle experiments. In contrast, the biomass composition differed between continuous light and day night cycle experiments (partly) due to starch respiration during the nights. This highlights the requirement of carbon partitioning in metabolic models.

2 Introduction

Among feedstocks for transportation fuel, the highest potential to overcome the prospective shortage [1, 2] is assigned to microalgae [3]. Advantages compared to terrestrial crops are the independence of arable land, faster areal biomass production rates and the accumulation of triacylglycerides (TAGs) to up to 50% of dry weight in some species [4-6]. TAGs can be extracted from biomass and converted to biodiesel by transesterification to be used as a pure fuel [4].

So far, no production chain solely based on biodiesel has been economically feasible [7, 8]. Improvements are required to overcome the following bottlenecks: low biomass concentrations; high water demand for regulating the temperature and compensating evaporation; high energy demand for mixing, harvesting and drying; high nutrient and CO_2 demand; complex controlling and high investment costs [7, 9]. All mentioned issues affect the energy, carbon and cost balance, which needs to be favorable to design a sustainable process [10].

A biorefinery approach using all products of the versatile metabolism of algae may turn the entire production chain profitable [3, 7, 8, 11]. The versatile metabolism offers products that can be used as food, feed, fine chemicals, antioxidants, pigments, pharmaceuticals and vitamins [12, 13]. Cultivation of algae is required on large scale to cover, especially, the demand for fuel, but still needs to be cost

competitive [14]. The main influences on algae growth and biomass accumulation are the available amounts of sunlight, water, CO_2, nitrogen and phosphorous, and the temperature [3, 15].

Current bottlenecks of microalgae cultivations can be identified with models gaining accurate productivity descriptions of the different biomass constituents to define the feedstock composition for the biorefinery. Models support the development of new technologies and optimization of processes for specific species, process designs and locations [16]. The predictions of an ideal model that can be used for the development, optimization and operation of microalgae cultivation systems are illustrated in Figure 1. Modeling of the microalgae metabolism is more complicated compared to modeling of the metabolisms of yeast, fungi or bacteria, since microalgal cells permanently adapt to light conditions and biological mechanisms are coupled with light distribution and hydrodynamics [16]. The expertise of biology, technology, scale-up, logistics and modeling needs to be combined to develop models, that demonstrate the environmental impact, productivities and economics of a production chain based on microalgae [10, 17].

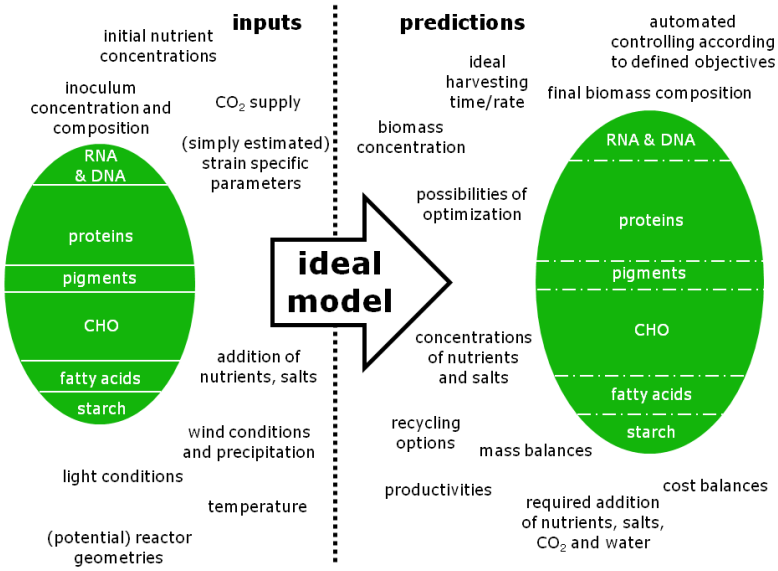

Figure 1: Illustration of the ideal model, which includes initial conditions as inputs, but also supply rates of e.g. nutrients and CO_2. These inputs may be manually varied or optimal values are automatically determined by the model according to defined objectives. All initial inputs and parameters can be independently estimated and have a strong biological or physical meaning. The ideal model predicts all desired information that is usable for process optimization and controlling or it even controls the process itself.

In contrast to ideal models, some existing models predict the productivity of the total biomass based on the availability of light without respect to carbon partitioning [14, 15, 18-21]. Energy costs for carbon fixation change with the composition of synthesized biomass [22]. Thus, these models are not suitable for stress conditions when accumulation of biomass constituents occurs, e.g. in highlight or under nitrogen depletion. Other models account for carbon partitioning with respect to different energy requirements, but oversimplify the available energy from photosynthesis [23, 24]. Still others consider TAG as the only biomass constituent, that is accumulated after nitrogen depletion [25] or do not include inter-conversion of biomass constituents [26].

Recently, a mechanistic model has been developed to estimate biomass, lipid and starch productivity for batch growth of *Scenedesmus sp.* under nitrogen depletion and constant light conditions [27]. As an improvement compared to previous models, this model describes the impact of nitrogen starvation on both photosynthesis and carbon partitioning. However, the applicability of this model to other algae species and non-optimal growth conditions have not been validated yet. Adjusting circumstances stepwise from optimal indoor towards outdoor conditions may help to identify crucial model parameters. If biological mechanisms are sufficiently understood, a model, including all of the abovementioned requirements, allows predictions of productivities for outdoors from simplified experiments. The incorporation of day night cycles and fluctuating temperatures are the most crucial steps, since commercial cultivations are performed outdoors and are, therefore, dependent on sunlight. Model predictions of productivities for different reactor geometries and environmental conditions are essential to plan and construct scale-ups.

In this study, the following research questions were investigated.

1. Which parameters and mechanisms need to be adjusted in the existing model by Breuer *et al.* to apply it to *C. littorale*?
2. Which physiological changes of simulated day night cycles can be observed compared to continuous light conditions and how can these be explained (model and biological agreement)?
3. Which additional parameters or changes of mechanisms need to be incorporated into the model to accurately describe growth and lipid productivity during day night cycles?
4. What is the effect of day night cycles on the predicted lipid and biomass productivity?

The model by Breuer *et al.* [27] was applied to *Chlorococcum littorale*. This microalgae was identified to be promising for TAG production [28-31], since it tolerates high CO_2 levels (60%) and grows to high biomass concentrations (80 g/L at 2000 µmol/m^2/s and 25 °C) [32, 33]. Strain specific model parameters were estimated from a batch cultivation of *C. littorale* under continuous light. Subsequently, the model was calibrated by fitting the maintenance requirement. The first step was taken to adjust the described model towards predicting outdoor biomass and lipid productivities by incorporation of light changes as a step function (16:8 h) and a mechanism for dark respiration. Effects of these simulated day night cycles were studied with another experiment, in this case, under changing light conditions (16:8 h) to obtain parameter values and calibrate the model. Model simulations were performed to estimate the effect of single parameters on the total biomass and TAG productivity.

3 Materials and Methods

3.1 Inoculum preparation and medium composition

The precultures of *Chlorococcum littorale* were grown for five to seven days in autoclaved Erlenmeyer flasks under continuous white light with an intensity of 60 µmol/m^2/s^1 and a temperature of 25±2°C. The salt-water-like medium contained 420.1 mM sodium chloride, 26.8 mM magnesium sulfate, 27.5 mM magnesium chloride, 10.2 mM calcium chloride, 10.7 mM sodium nitrate (150 mg N-NO_3^-/L), 11.7 µM EDTA-Fe(III)-Na-salt, 0.7 mM dipotassium phosphate and 0.3 mM monopotassium phosphate. One milliliter of trace element stock solution ($Na_2EDTA{\cdot}2H2O$ 0.19 g/L, $ZnSO_4{\cdot}7H_2O$ 0.022 g/L, $CoCl{\cdot}6H_2O$ 0.01 g/L, $MnCl_2{\cdot}2H_2O$ 0.148 g/L, $Na_2MoO_4{\cdot}2H_2O$ 0.06 g/L, $CuSO_4{\cdot}5H_2O$ 0.01 g/L) was added per liter of medium.

3.2 Reactor set-up and conditions

The batch cultivations were performed in a rectangular-shaped flat panel air-lift photobioreactor (0.27 m x 2.45·10^{-2} m x 0.73 m (w x d x h)) with a working volume of approximately 4.2 L. The reactor was autoclaved prior to usage. The cultivation medium equaled the one described in 3.1, except for the nitrate concentration (approximately 100 g N-NO_3/L). The medium was pumped into the reactor through a sterile filter (0.2 µm).

One batch cultivation with continuous light (24 h, 542.5 µmol/m^2/s^1) and another one with simulated day night cycles (16:8, 530.7 µmol/m^2/s^1) were performed. Both experiments were nitrogen run-outs, meaning that nitrogen was initially added and depleted during the cultivation time. The initial biomass concentrations were 0.25 g/L and 0.19 g/L for the continuous light and day night cycles, respectively. The unilaterally supplied light was red and blue and the amount of outgoing light was neglected for calculations, since it was below 10% of the incident light intensity after one day of cultivation in the continuous light run. The outgoing light of the day night cycles could not be measured due to the construction that protected the reactor from external light. The air flow was set to 2000 mL/min including a default CO_2 fraction of 2%. The pH was regulated at a value of 7.0 by the CO_2 supply. The temperature was manually regulated to approximately 25°C. The gas, pH and temperature setting were equal for continuous light and day night cycles. As soon as excessive amounts of foam were visible, 40% antifoam solution was diluted in water and injected, until the foam decreased. Approximately 1 mL and 2 mL of 40% antifoam were added in the continuous light and day night cycle experiment, respectively, distributed over the cultivation time. Samples were taken once to twice a day during the continuous light run and in selected nights during simulated day night cycles. The total sampling volume was below 0.8 L, while no substantial evaporation losses were observed. Cultivations were stopped, when the biomass concentration was not increasing for at least two days (continuous light: 232 h, day night cycles: 336 h).

3.3 Biomass analyzes

The biomass composition (as percentage of dry weight (DW)) was analyzed at selected sampling points for its content of triacylglycerides, starch and carbohydrates (including starch). All measurements were performed as technical duplicates unless stated differently.

3.3.1 Dry weight

The dry weight concentration was determined gravimetrically by filtering a defined culture volume (1-4 mL diluted with 20 mL 0.5 M ammonium formate) through prewashed and weighed glass microfiber filters (θ55 mm, pore size 0.7µm, Whatman International Ltd, Maidstone, UK). The filter with biomass was washed with another 20 mL of 0.5 M ammonium formate. After drying the filter (>24 hours, 105°C), the weight difference to empty filters was determined and normalized to one liter of culture volume.

3.3.2 Triacylglycerides

Fatty acid extraction, separation of triacylglycerides and quantification were performed as described by Breuer *et al.* [34]. Briefly, freeze dried biomass (10 mg) was disrupted by bead beating and the total lipids were extracted with chloroform:methanol (2:2.5). The non-polar lipids were separated using a solid phase extraction column washed with hexane:diethylether (7:1). After transesterification, the fatty acids were quantified by gas chromatography.

3.3.3 Starch

The starch content of homogenized biomass was determined using an α-amylase and amyloglucosidase based starch assay (Megazyme K-TSTA 07/11, Ireland).

Freeze dried biomass (10 mg) was disrupted in bead beating tubes (Lysing Matrix E; MP Biomedicals) in presence of 1 mL 80% (v/v) ethanol (3 cycles: 60 s, 6000 rpm, 120 s break; PRECELLYS® 24). After transferring the content of the bead beating tube to a fresh glass tube and rinsing with 80% (v/v) ethanol (4x1 mL), the suspension was incubated at 80-85°C (5 min). Another 5 mL ethanol (80%) was added prior to mixing. Starch was precipitated by centrifugation (10 min, 2500 rpm; 1580R, LABOGENE). The supernatant was discarded. Subsequently, the procedure was performed according to the manufacturer's instructions (Megazyme K-TSTA 07/11, Ireland, b, step 4 and 5) with the exception, that after hydrolysis, 0.1 mL supernatant of the samples and the glucose standards were directly used for the quantification of the glucose concentration (step 8-10). The absorption was measured spectrophotometerically at the wavelength 510 nm. All solutions were freshly prepared and no sodium azide was added. The hydrolyzed samples were measured against a D-glucose calibration series.

3.3.4 Total carbohydrates

The estimation of the total carbohydrate content is based on acid hydrolysis, followed by the spectrophotometerical quantification of glucose monomers colored by treatment with phenol and concentrated acid [35]. The procedure is described below.

Freeze dried biomass (1 mg) and the positive control starch were each dissolved in 2.5 M HCl (0.5 mL). After incubating the sample in a boiling water bath for three hours and cooling down to room temperature, 2.5 M NaOH (0.5 mL) are added to neutralize the suspension. The suspension was mixed, and 50 µL were immediately transferred to a fresh tube. Ultrapure water was added (450 µL) to the biomass and starch sample. Diluted phenol (5% (v/v), 500 µL) was added to both samples and the glucose calibration series. The last steps of the procedure are the addition of 2.5 mL concentrated sulphuric acid, incubation of 10 min at room temperature and 30 min at 35°C. The absorption was measured at 483 nm against a glucose-free sample as a blank.

Remark: Some measurements resulted in negative concentrations or concentrations of carbohydrates other than starch close to zero. These values were not taken into account for parameter estimation, since they do not agree with the presence in the cell wall [36].

3.4 Dissolved nitrogen

A culture sample (1-2 mL) was centrifuged to collect the supernatant (5 min, 13300 rpm, Micro Star 17R, VWR®). The nitrate concentration of the supernatant was determined by using the standard method of the Seal analytical AQ2 nutrient analyzer (SEAL Analytical Inc., USA) according to the manufacturer's instructions.

3.5 Absorption spectrum

The optical density of the culture suspension was measured at 750 nm (OD_{750nm}) by a spectrophotometer (light path: 1 cm, DR 5000, HACH LANGE). The sample was diluted to an OD_{750nm} of 0.3 to 0.8 to avoid saturated absorption. The absorption spectrum of the diluted culture sample was recorded in a precision cell (light path: 2 mm, Hellma® Analytics) using the fiber optic spectrometer AvaSpec-2048 (avantes) with the light source AvaLight-Hal.

4 Results and discussion

4.1 Experimental results

Nitrogen run-out batches of *Chlorococcum littorale* were inoculated at biomass concentrations of 0.25 g/L in continuous light (cont) and 0.19 g/L in day night cycles (dn; 16:8 h). At the time of inoculation, the nitrate concentrations were 100 mg $N\text{-}NO_3^-$/L (cont) and 105 mg $N\text{-}NO_3^-$/L (dn). The onset of nitrogen starvation was considered at the point in time when the nitrate concentration approached zero. This was observed after approximately 25 h (cont) and 40 h (dn) at biomass

concentrations of 1.1 g/L (cont) and 1.6 g/L (dn). At this point, all existing biomass was considered to be nitrogen repleted and is further on called reproducing biomass.

The maximum time-averaged triacylglyceride (TAG) yields were estimated as 0.08 g TAG/L/d (cont) and 0.04 g TAG/L/d (dn) based on TAG produced after the inoculation. The highest total biomass concentrations observed were 3.1 g/L after 160 h (cont) and 3.3 g/L after 256 h (dn) of cultivation time (Figure 2 a, b). During nitrogen depletion, the increase in biomass concentration (Figure 2 a, b) was mainly due to TAG and starch accumulation under both light conditions (Figure 2 c, d). The continuous light culture reached a maximum TAG and starch content of 14.5% and 37.3% (after 138 h), respectively. The content of carbohydrates other than starch was fluctuating around 30.0% after nitrogen depletion (neglecting outliers). In the day night cycle experiment, the maximum TAG content was lower (13.1%) and the maximum starch content was higher (42.4%) at the end of the cultivation (after 336 h) than in continuous light conditions. The average content of carbohydrates other than starch was 15.1% after nitrogen depletion in day night cycles (neglecting outliers). Thus, the maximum content of total carbohydrates and TAG were both higher under continuous light conditions than in day night cycles, while the amount and fraction of reproducing biomass was lower.

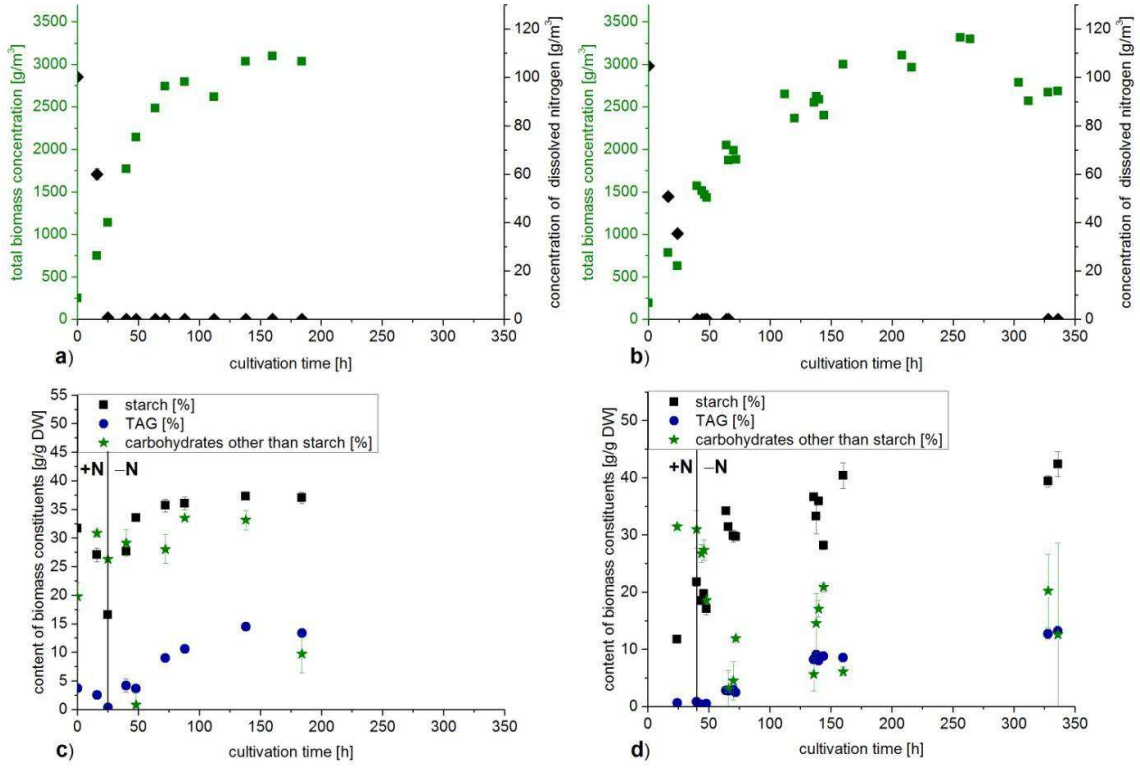

Figure 2: Total biomass concentration (green squares) and dissolved nitrogen ($N\text{-}NO_3^-$) concentrations (black diamonds) in continuous light (a) and day night cycles (b). The biomass composition as starch (black squares), TAG (blue circles) and carbohydrates other than starch (green stars) is shown in continuous light (c) and day night cycles (d). The onset of nitrogen depletion is indicated by the black line (c, d). All data points are the average of two technical replicates except for the first value of starch and TAG concentration and the last value of starch under continuous light conditions. In some cases, the error bars representing single measurements are covered by a symbol.

The amount of generated biomass after inoculation was plotted against the amount of supplied photons to estimate the effect of nights compared to continuous light conditions (Figure 3). No difference in the overall yields of biomass on photons was observed between continuous light and day night cycles (Figure 3a). Nevertheless, biomass was degraded during nights, accounting for a decrease of 5 to 20% of the dry weight concentration before the night. The 'biomass loss' was compensated the next day. This suggests a higher photosynthetic efficiency in day night cycles than in continuous light. However, the evaluation of the energy content of the biomass is required to estimate the photosynthetic efficiency, since TAG and protein synthesis utilize more energy per carbon atom than carbohydrate synthesis [37]. The biomass composition was analyzed for both the continuous light experiment (cont: 48 h) and the day night cycle experiment (dn: 64 h) after the input of approximately 3800 mol photons/m^3. At the mentioned time points, the measured TAG concentrations were 68.5 g TAG/m^3 (cont) and 50.3 g TAG/m^3 (dn, Figure 3b), while the starch concentrations were equal in both cultivations (Figure 3c). Instead of fixing carbon as 18.2 g TAG/m^3, 44.3 g STA/m^3 could have been produced based on the same energy input. The difference of TAG concentrations results from a difference in the amount of energy partitioned to TAG synthesis (13.7 mol photons/m^3, according to theoretical maximum yields in Table 2). This illustrates the importance of carbon partitioning in metabolic modeling of microalgae cultivations [22, 27, 37], since the composition changes due to the presence of nights.

The total amount of energy incorporated into the biomass cannot be evaluated based on the presented data due to uncertainties in the content of carbohydrates other than starch and in the composition of reproducing biomass in day night cycles. The total carbohydrate measurement was not reliable, since it showed unstable measurement errors. The biomass composition was only estimated under nitrogen replete conditions in continuous light. Differences in the composition of reproducing biomass lead to the deviation of the energy requirement for synthesis from the theoretical maximum yield (Table 1). A higher fraction of energy-rich components, e.g. TAG and proteins, causes a lower maximum yield of reproducing biomass on photons [23]. The calculated cellular nitrogen content (consumed amount of $N\text{-}NO_3^-$ plus amount of $N\text{-}NO_3^-$ in inoculum per existing biomass) and the absorption cross section indicate that the composition of reproducing biomass in day night cycles differed from the one in continuous light. The maximum amount of $N\text{-}NO_3^-$ taken up by the biomass was 9.7% g $N\text{-}NO_3^-$/g biomass (cx) in continuous light occurring with the maximum absorption cross section of 0.138 m^2/g cx. Similar slopes of the absorption cross section and the cellular nitrogen content were observed, when plotting both values against the cultivation time separately for different light conditions (Supplementary material S 3). However, the correlation between the absorption cross section and the cellular nitrogen content was different under and shortly after nitrogen replete conditions in day night cycles, since nitrogen was taken up

over night. Therefore, the maximum measured absorption cross section (0.170 m^2/g cx) was reached at a cellular nitrogen content of 7.8% g N-NO_3^-/g cx. The nitrogen assimilation over night in combination with an increase of the absorption cross section is in agreement with the synthesis of nitrogen containing compounds, such as proteins, during nights as observed in outdoor cultivations of *Spirulina* sp. [38]. The high energy demand for pigment and protein production [22] can be supplied by respiration of carbohydrates during nights [38]. If pigments and photosynthetic proteins are synthesized and repaired during the night, an increased photosynthetic rate and efficiency after the night seem reasonable, but was not experimentally observed due to exclusive sampling during nights. The major amount of cellular nitrogen is incorporated into proteins and pigments [22]. Thus, the lower cellular nitrogen content of reproducing biomass indicates the lower content of proteins or pigments correlated with a reduced energy requirement for synthesis of reproducing biomass. Therefore, the energy density of the total biomass in day night cycles could have been lower, even though the fraction of reproducing biomass was considered to be higher than in continuous light.

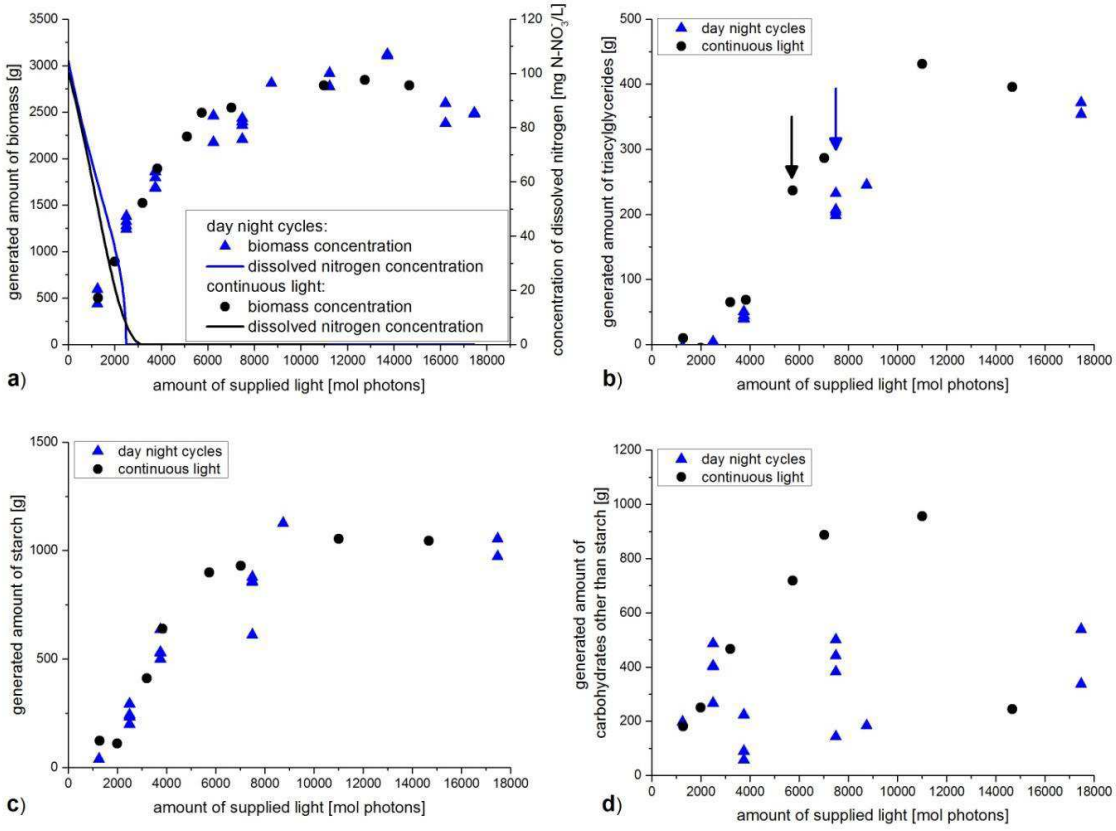

Figure 3: Generated amount of total biomass (a), triacylglycerides (b), starch (c) and carbohydrates other than starch (d) versus the amount of supplied photons in the continuous light (black circles) and the day night cycle experiment (blue triangles). The dissolved nitrogen concentrations (a, solid lines) and the maximum TAG yields (b, arrows) are indicated for continuous light (black) and day night cycle experiments (blue). All data points are the average of two technical replicates except for the first value of starch and TAG concentration and the last value of starch under continuous light conditions.

Additionally, the exact time point of the onset of nitrogen depletion and, thus, the concentration of reproducing biomass was uncertain, since the sampling time did not match the onset of nitrogen depletion. However, the effect of nights on the biomass composition and concentrations needs to be further evaluated. More information about physiological effects of nights was obtained by examining the trend of the biomass composition during nights (Figure 4). The observed biomass loss over night was >68% accounted as starch, while no clear trend of carbohydrates other than starch could be observed. TAG degradation yields more energy per carbon atom, but its optimal value for return of investment in terms of adenosine triphosphate (ATP) equivalents (60.7%) is lower than the one of carbohydrates (65.3-66.7%) [39]. In conclusion, the degradation of carbohydrates to supply energy for maintenance is more efficient than the degradation of TAG considered as a cycle of synthesis during days and degradation during nights. The TAG content of *C. littorale* fluctuated during nights, which was also observed for the total lipid content of *Chlorella pyrenoidosa* [40].

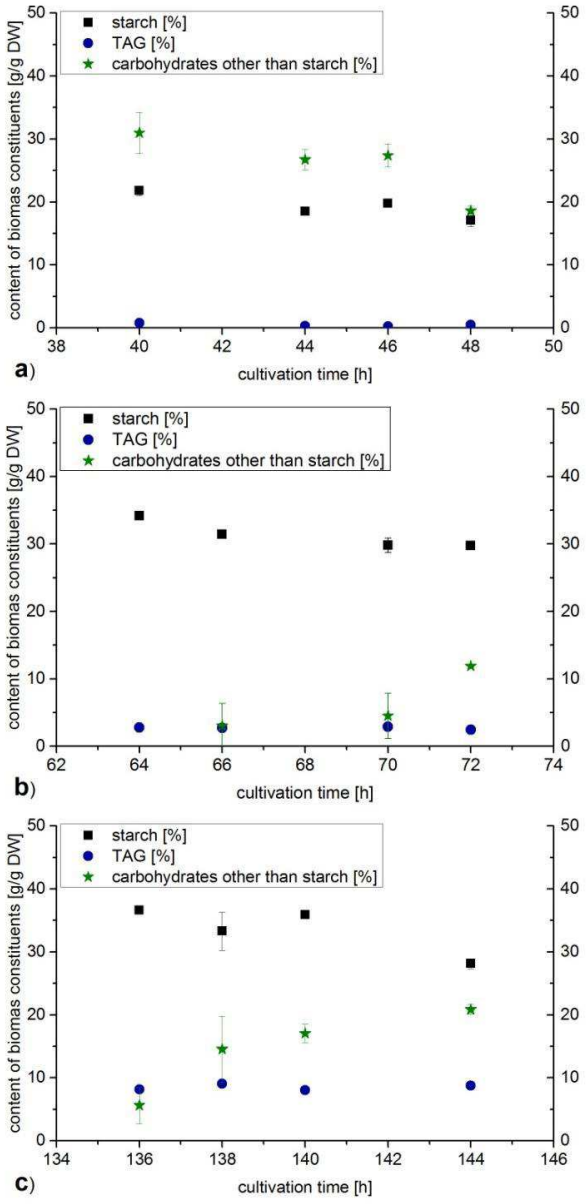

For both the continuous light and day night cycle experiment, the TAG productivities and contents were low compared to values reported for *Chlorococcum littorale* and other lipid accumulating algae species in the literature [31, 41]. Reasons for the low TAG and biomass productivity may be inefficient mixing in the reactor and relatively low volumetric light supply leading to insufficient stress conditions. TAG productivity in *C. littorale* could be improved by e.g. lower oxygen concentrations [31].

Figure 4: Fractions of starch (black squares), TAG (blue circles) and carbohydrates other than starch (green stars) in dry weight during selected nights (a, b ,c) of the day night cycle experiment. All data points are the average of two technical replicates. In some cases, the error bars representing single measurements are covered by a symbol.

4.2 Model description

A mechanistic model to predict the productivity of triacylglycerides (TAG) using oleaginous microalgae in nitrogen run-out batches was designed by Breuer *et al.* [27]. The model distinguishes the available energy through photosynthesis and carbon partitioning. The available energy is estimated based on strain specific characteristics (absorption cross section, maximum specific growth rate, and maintenance requirement), light conditions (incident light intensity and light path) and the biomass composition. Different biomass constituents, namely, reproducing biomass (X), TAG, carbohydrates other than starch (CHO), and starch (STA) are generated at distinct biomass specific production rates. Inherent photosynthetic yields for each biomass constituent are taken into account to estimate the amount of synthesized biomass constituents on the basis of available energy. Reproducing biomass is defined as the biomass fraction, which is produced during the nitrogen replete phase (Figure 5: b). Thus, reproducing biomass includes nitrogen containing compounds (e.g. pigments and proteins) as well as carbohydrates. The terms TAG, CHO and STA only refer to biomass, which is produced in the nitrogen deplete phase at rates depending on the existing biomass composition. The model has been validated for *S. obliquus* during nitrogen starvation under continuous light conditions. A detailed description of the model can be found in the Appendix (6.1).

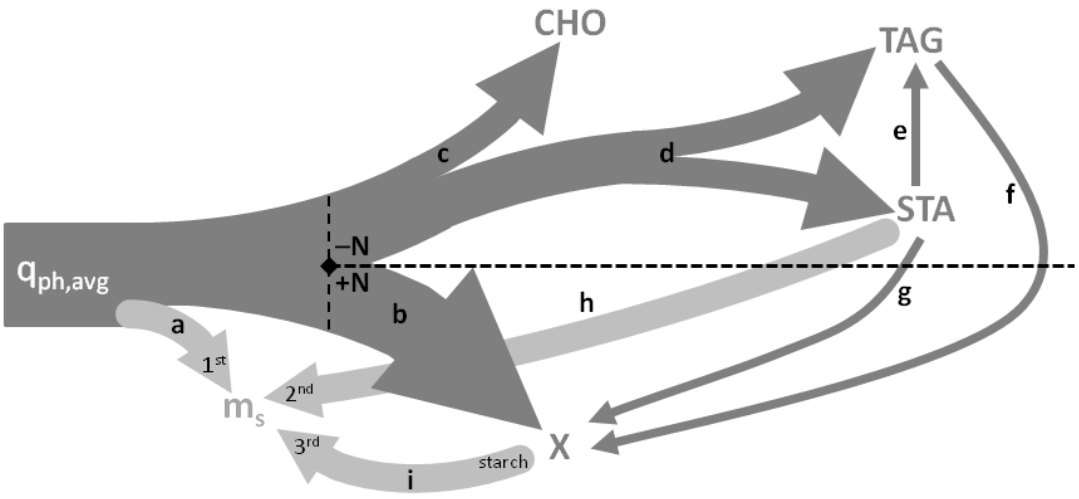

Figure 5: Carbon partitioning. The available energy from absorbed photons after subtracting heat dissipation ($q_{pg,avg}$) is first used to cover the maintenance requirement (m_s, a). All remaining energy drives the production of reproducing biomass (X) under nitrogen replete conditions (b). Additionally, triacylglycerides (TAGs, f) and starch outside of X (STA, g) are converted to X, if these constituents are present. During nitrogen starvation the maintenance requirement (m_s) still needs to be covered. Energy is partitioned to carbohydrates other than starch (CHO), TAG and STA. The highest priority is keeping the CHO content of the total biomass constant (c). Carbon partitioning between TAG and STA (d) is estimated empirically as a correlation of the cellular nitrogen content. The inter-conversion of STA to TAG occurs, when Q drops below a certain value (e). Insufficient irradiance causes STA degradation for maintenance (h). Additionally, f and g occur, if TAG and STA are present, respectively. If no STA is available, starch out of reproducing biomass is degraded (i). For more details see 6.1 for the continuous light model and 4.2.1 for day night cycle extensions.

In the present study, the model is applied to growth and product formation of *Chlorococcum littorale* under continuous light conditions. The inter-conversion of STA and TAG to reproducing biomass (Figure 5: g and f, respectively) was included. This model extension allows a more accurate description of photosynthesis and carbon partitioning, if the initial biomass composition differs from reproducing biomass. Additionally, day night cycles were simulated taking changing light intensities and dark respiration of starch (Figure 5: h) into account. For the model evaluation experimental data (4.1) have been used.

4.2.1 Model extension for simulated day night cycles

The first step of adjusting the continuous light model to day night cycles is incorporating the light change dependent on cultivation time. In this approach, the light is regulated as a step function, which starts with a light period. The light intensity is set to I_0, if the evaluated time point during the day is lower than the time duration of light hours per day (dlds, (Eq. 1) with t: cultivation time, nd: number of day, dds: duration of day).

$$I(t) = \begin{cases} I_0 & \text{if } (t - nd \cdot dds) < dlds \\ 0 & \text{if } (t - nd \cdot dds) \geq dlds \end{cases} \quad \text{(Eq. 1)}$$

During the dark phase, no energy source is present, so the biomass specific photosynthetic rate (Eq. 21) equals zero. In this case, all biomass constituents are degraded at the same rates according to the first term of the equations (Eq. 25), (Eq. 27), (Eq. 30) and (Eq. 31). The degradation rate of each biomass constituent separately would cover the entire maintenance requirement. Furthermore nitrogen containing compounds of reproducing biomass would be broken down and release nitrate (Eq. 26). In conclusion, these equations do not hold to simulate the actual situation, if the energy required for maintenance cannot be supplied by light.

The first term, which includes photosynthetic energy supply and maintenance requirement, is removed from the equations (Eq. 25), (Eq. 27),(Eq. 30) and (Eq. 31), if the maintenance requirement is not covered. Instead, the specific maintenance rate for reproducing biomass was incorporated as starch degradation lowering the biomass specific production rate of STA (Eq. 2).

$$qSTA = \begin{cases} -r_{STA/TAG} - r_{STA/X} - \frac{m_s \cdot Q}{Q_{max}} \cdot \frac{yATPph}{yATPSTA} & \text{if } STA > 0 \text{ and } q_{ph,avg} < \frac{m_s \cdot Q}{Q_{max}} \\ 0 & \text{if } STA = 0 \text{ and } q_{ph,avg} < \frac{m_s \cdot Q}{Q_{max}} \end{cases} \quad \text{(Eq. 2)}$$

The specific maintenance requirement for reproducing biomass in terms of photons is translated to the demand as starch using the yield of ATP on photons (yATPph) and the yield of ATP on starch (yATPSTA). Preferentially, accumulated starch (STA) is assumed to be degraded. If no STA is present,

starch still represents a fraction of reproducing biomass (XSTAX). Thus, this fraction can be degraded to cover maintenance requirement (Eq. 3) using the same term as described for STA degradation (Eq. 2).

$$qX = \begin{cases} r_{STA/X} \cdot yXSTA + r_{TAG/X} \cdot yXTAG & \text{if } STA > 0 \text{ and } q_{ph,avg} < \dfrac{m_s \cdot Q}{Q_{max}} \\ r_{TAG/X} \cdot yXTAG + STAinXdeg & \text{if } STA = 0 \text{ and } q_{ph,avg} < \dfrac{m_s \cdot Q}{Q_{max}} \end{cases} \quad \text{(Eq. 3)}$$

$$\text{with } STAinXdeg = -\frac{m_s \cdot Q}{Q_{max}} \cdot \frac{yATPph}{yATPSTA}$$

The degradation of starch out of reproducing biomass causes a change in the reproducing biomass composition, which was by definition constant before. The former definition of the cellular nitrogen content (Eq. 19) does not hold. Since no nitrogen containing compounds are degraded, the new definition of the cellular nitrogen content takes the concentration of reproducing biomass before the night into account (Eq. 4).

$$Q = Q_{max} \cdot \frac{X - degSTA}{c_x} \quad \text{(Eq. 4)}$$

Therefore, the existing reproducing biomass concentration (X) is corrected for the amount of starch, which has been degraded from reproducing biomass (degSTA, negative value) during the present night. At the same time, the total biomass concentration (c_x) takes the decrease of starch into account. Thus, the cellular nitrogen content may exceed Q_{max} leading to a quantum yield higher than one after nights. In this case, the quantum yield is set to one (Eq. 5), since the energy used by the cells cannot exceed the supplied energy.

$$QY = \min\left\{\left(1 - \frac{Q_{min}}{Q}\right) \cdot \left(1 - \frac{Q_{min}}{Q_{max}}\right)^{-1}; 1\right\} \quad \text{(Eq. 5)}$$

As soon as light is available, a certain fraction (f_{part}) of the available energy is assumed to be partitioned to starch to restore the degraded amount of reproducing biomass (Eq. 6). This leads to the same composition of reproducing biomass after the replacement of starch as before the night. The remaining energy is partitioned according to the same priorities as during the continuous light cultivation giving the following biomass specific production rates for reproducing biomass (Eq. 7), CHO (Eq. 8), TAG (Eq. 9) and STA (Eq. 10). Only the condition for the biomass specific production of

CHO is corrected for the degraded amount of starch (Eq. 8) analogous to the correction of the cellular nitrogen content (Eq. 4).

$$qX = \begin{cases} \overbrace{yXph \cdot \left(q_{ph,avg} - \frac{m_s \cdot Q}{Q_{max}}\right) \cdot (1 - f_{part})}^{qX1} + r_{TAG/X} \cdot yXTAG + STAinXdeg & \\ & \text{if } N > 0 \text{ and } q_{ph,avg} > \frac{m_s \cdot Q}{Q_{max}} \\ STAinXdeg & \text{if } N = 0 \text{ and } q_{ph,avg} > \frac{m_s \cdot Q}{Q_{max}} \end{cases} \quad \text{(Eq. 7)}$$

$$\text{with } STAinXdeg = ySTAph \cdot \left(q_{ph,avg} - \frac{m_s \cdot Q}{Q_{max}}\right) \cdot f_{part}$$

$$qCHO = \begin{cases} \left(\left(q_{ph,avg} - \frac{m_s \cdot Q}{Q_{max}}\right) \cdot (1 - f_{part}) - \frac{qX1}{yXph}\right) \cdot yCHOph & \text{if } xCHO \leq XCHO \\ 0 & \text{if } xCHO > XCHO \end{cases} \quad \text{(Eq. 8)}$$

$$\text{with } xCHO = \frac{XCHOX \cdot (X - degSTA) + CHO}{c_x}$$

$$qTAG = \left(\left(q_{ph,avg} - \frac{m_s \cdot Q}{Q_{max}}\right) \cdot (1 - f_{part}) - \frac{qX1}{yXph} - \frac{qCHO}{yCHOph}\right) \cdot f_{TAG} \cdot yTAGph + r_{STA/TAG} \cdot yTAGSTA - r_{TAG/X} \quad \text{(Eq. 9)}$$

$$qSTA = \left(\left(q_{ph,avg} - \frac{m_s \cdot Q}{Q_{max}}\right) \cdot (1 - f_{part}) - \frac{qX1}{yXph} - \frac{qCHO}{yCHOph}\right) \cdot (1 - f_{TAG}) \cdot ySTAph - r_{STA/TAG} - r_{STA/X} \quad \text{(Eq. 10)}$$

According to (Eq. 26) an increase of the dissolved nitrogen concentration occurs, if the biomass specific production rate of reproducing biomass is negative. Further on, restoring starch in reproducing biomass as defined in (Eq. 7) would contribute to nitrogen consumption without increasing the cellular nitrogen content. Both issues are overcome by redefining the biomass specific nitrogen consumption rate with a correction for the rate of restoring starch (STAinXdeg, (Eq. 11)).

$$qN = \begin{cases} -(qX - STAinXdeg) \cdot Q_{max} & \text{if } qX \geq 0 \\ r_{TAG/X} \cdot yXTAG & \text{if } qX < 0 \end{cases} \quad \text{(Eq. 11)}$$

After all starch is restored in reproducing biomass, f_{part} is set to zero (Eq. 37), thus, the same partitioning as described for the continuous light cultivation occurs.

$$f_{part} = \begin{cases} f_{part} & \text{if } degSTA < 0 \\ 0 & \text{if } degSTA = 0 \end{cases} \quad \text{(Eq. 12)}$$

4.2.2 Parameter estimation

The parameters used in the model can be divided in three categories: theoretical yields on photons and conversion yields (6.2.1), experimentally estimated parameters (6.2.2), and fitted parameters (6.2.3). All parameters with equal values for continuous light and day night cycles are summarized in Table 2 (p. 30) and parameters with differing values in Table 1 (p. 15).

Table 1: Initial conditions and estimated parameters differing between continuous light and simulated day night cycle cultivations.

condition	continuous light	day night cycle	unit
cx_0	248.3	190.0	$\frac{\mathrm{g\ DW}}{\mathrm{m^3}}$
X_0	192.3	147.2	$\frac{\mathrm{g\ DW}}{\mathrm{m^3}} \cdot \frac{\mathrm{Q}}{\mathrm{Q_{max}}}$
TAG_0	9.2	7.0	$\frac{\mathrm{g\ TAG}}{\mathrm{m^3}}$
STA_0	46.8	34.5	$\frac{\mathrm{g\ STA}}{\mathrm{m^3}}$
CHO_0	0.0	0.0	$\frac{\mathrm{g\ CHO}}{\mathrm{m^3}}$
$N\text{-}NO_3$	100.2	104.7	$\frac{\mathrm{g\ N}}{\mathrm{m^3}}$
pA	0.00850	0.00865	–
pB	1.3860	1.2255	–
cd	200.0	350.0	h
I_0	$542.5 \cdot 10^{-6}$	$530.7 \cdot 10^{-6}$	$\frac{\mathrm{mol\ photon}}{\mathrm{m^2 \cdot s}}$
dds	24.0	24.0	h
dlds	24.0	16.0	h
XCHO	30.0	15.1	$\frac{\%\ \mathrm{g\ CHO}}{\mathrm{g\ DW}}$
arep	0.138	0.170	$\frac{\mathrm{m^2}}{\mathrm{g}}$
Q_{max}	9.7	7.8	$\frac{\%\ \mathrm{g\ N}}{\mathrm{g\ DW}}$
$q_{ph,max,rep}$	$1.18 \cdot 10^{-5}$	$1.52 \cdot 10^{-5}$	$\frac{\mathrm{mol\ photon}}{\mathrm{g\ DW} \cdot \frac{\mathrm{Q}}{\mathrm{Q_{max}}} \cdot \mathrm{s}}$
f_{part}	0.00	0.32	–

4.3 Continuous light model applied to *Chlorococcum littorale*

The model developed by Breuer *et al.* to predict biomass and TAG productivities of *Scenedesmus obliquus* under continuous light conditions [27] was applied to *Chlorococcum littorale.* No adjustments of model mechanisms were required besides the conversion of accumulated TAG and starch (STA) to reproducing biomass (X) due to inoculation with non-nitrogen repleted biomass and parameters were estimated as described in 4.2.2. The estimated maintenance requirement of $6.25 \cdot 10^{-7}$ mol photon/g X/s was an order of magnitude higher than the maintenance requirement estimated for *S. obliquus* ($2.78 \cdot 10^{-8}$ mol photon/g X/s). The experimentally determined maintenance requirement of *Chlamydomonas reinhardtii* is reported as $2.97 \cdot 10^{-7}$ mol photon/g DW/s [23] taking into account the yield of ATP on photons (0.375 ATP/photon). The maintenance requirement estimated in this study by fitting the model is considered to be more realistic than the one assumed by Breuer *et al.*, since it is in the same order of magnitude as the experimental determined one. The estimated maintenance requirement is dependent on the implemented mechanisms and parameter values (see Table 1 (p. 15) and Table 2 (p. 31)) and, therefore, not necessarily in agreement with the actual maintenance requirement.

After fitting the maintenance requirement, the ordinary differential equations (Eq. 13)-(Eq. 17) describing the production rates of reproducing biomass, TAG, STA and CHO as well as the consumption rate of nitrogen were solved in Matlab (ode45 (cont), ode23s (dn)) to simulate the continuous light cultivation. The outputs CHO and STA were corrected according to the equations (Eq. 39) and (Eq. 40) to generate experimentally measurable data. The model showed a good fit to the experimental observed data as shown in Figure 6 and indicated by the R-squares (R^2(cx)=0.988, R^2(X)=0.848, R^2(TAG)=0.958, R^2(STAm)=0.730, R^2(CHOm)=0.239 and R^2(N)=0.893). Solely, the maximum biomass specific growth rate and, therefore, the biomass specific photosynthetic rate seemed to be underestimated in the beginning of the cultivation. This resulted in slower biomass accumulation and nitrate consumption.

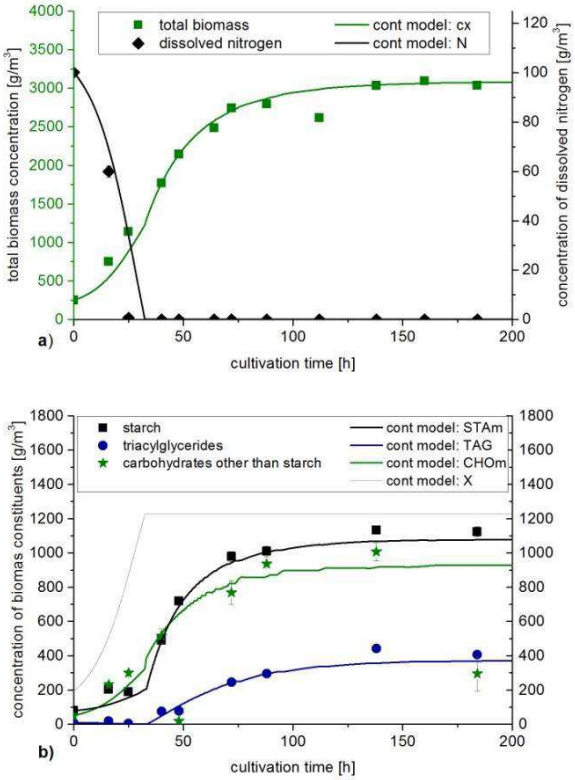

Figure 6: Model simulation of the continuous light experiment. Solid lines represent the model output and symbols represent the experimentally obtained data. Concentrations of the total biomass (cx, green squares, green line) and nitrogen (N(-NO_3^-), black diamonds, black line) are shown in (a). The concentrations of the measurable amount of starch (STAm, black squares, black line) and carbohydrates other than starch (CHOm, green stars, green line) as well as the concentration of triacylglycerides (TAG, blue circles, blue line) and the simulated concentration of reproducing biomass (X, grey line) are presented in (b). All data points are the average of two technical replicates except for the first value of starch and TAG concentrations and the last value of starch. In some cases, the error bars representing single measurements are covered by a symbol.

The absorption cross section under nitrogen replete conditions and the nitrogen content of nitrogen replete cells were similar for both algae species *C. littorale* and *S. obliquus*. The CHO content of biomass after the onset of nitrogen depletion was found to be relatively constant in *S. obliquus* [42], which was also assumed for *C. littorale* based on the obtained measurements.

The major differences between *C. littorale* (C.l.) and *S. obliquus* (S.o.) were found in the following parameters: The biomass specific photosynthetic rate (C.l.: 0.4251 mol photons/g X/h, S.o.: 0.0642 mol photons/g X/h) was calculated based on the biomass specific growth rate (C.l.: 1.7 d^{-1}, S.o.: 3.0 d^{-1}). The correlation of the partition coefficient of carbon to TAG and starch synthesis (pA and pB) shows, that more carbon atoms are partitioned to TAG in *C. littorale* than in *S. obliquus* at the same cellular nitrogen content. Nevertheless, the biomass accumulation stopped in the culture of *C. littorale*, before high amounts of TAG could be accumulated at the minimum nitrogen content (3.7%) and the amount of degraded starch was neglectable. The final biomass concentration of *S. obliquus* was approximately 10,000 g/m^3 after 200 h, whereas *C. littorale* grew to a biomass concentration of only 3,000 g/m^3. The difference is caused by the higher tolerance of *S. obliquus* towards low cellular nitrogen contents (1.2%.). *S. obliquus* showed conversion of starch into TAG at cellular nitrogen concentrations below 1.4% with a stable reaction rate. The combination of conversion of starch to TAG and the high biomass concentration resulted in the high maximum TAG yield on photons (0.144±0.004 g TAG/mol photon) [42] compared to *C. littorale* (0.04 g TAG/mol photons).

In conclusion, the model showed to hold for *C. littorale* following the description of initial parameter estimation by Breuer *et al.*, even though several parameters largely differed. However, for the model validation biological replicates of the cultivation are required and several parameters need to be estimated more precisely, namely, the carbohydrate content; the composition of reproducing biomass; the maximum biomass specific photosynthetic rate and the correlation of the coefficient for carbon partitioning between TAG and starch to the cellular nitrogen content.

4.4 Evaluation of the model extension for day night cycles

The model described in 6.1 was extended to become suitable for day night cycles. The extension is based on the implementation of light changes and respiration of biomass during the nights. The modeled dark respiration solely depends on the cellular nitrogen content of the existing biomass, which is often used as a proxy to predict physiological effects in microalgae cultivations [16]. In the model, the entire energy for maintenance is supplied by starch degradation. Most parameters obtained in continuous light experiments were used to model the day night cycles. Only the following inputs were adjusted according to the measurements obtained in day night cycles as described in 4.2.2.: the initial concentrations of the biomass constituents, the maximum cellular nitrogen content, the maximum absorption cross section, the content of carbohydrates other than starch after nitrogen depletion and the correlation of the partition coefficient f_{TAG} to the cellular nitrogen content.

Figure 7 shows the simulation and experimental data of the performed day night cycles. On average, the trends of the total biomass, TAG, measurable starch and carbohydrates other than starch concentrations roughly matched the experimental observations. Nevertheless, starch production is underestimated during the nitrogen replete phase and overestimated shortly after the onset of nitrogen depletion leading to an overprediction of approximately 20% of starch ($t > 60$ h). The overestimation is likely to be caused by the underestimated degradation of starch during the nights. The consumption rate of dissolved nitrogen was underestimated and the reproducing biomass is accumulated faster than predicted. This underestimation was considered to be partly caused by an underestimation of the biomass specific growth rate, or the underestimation of the maximum absorption cross section, or a combination of both. The dark respiration due to the maintenance requirement was resulting in a lower biomass loss than experimentally observed. Potential reasons that caused the higher dark respiration rate than predicted need to be further investigated.

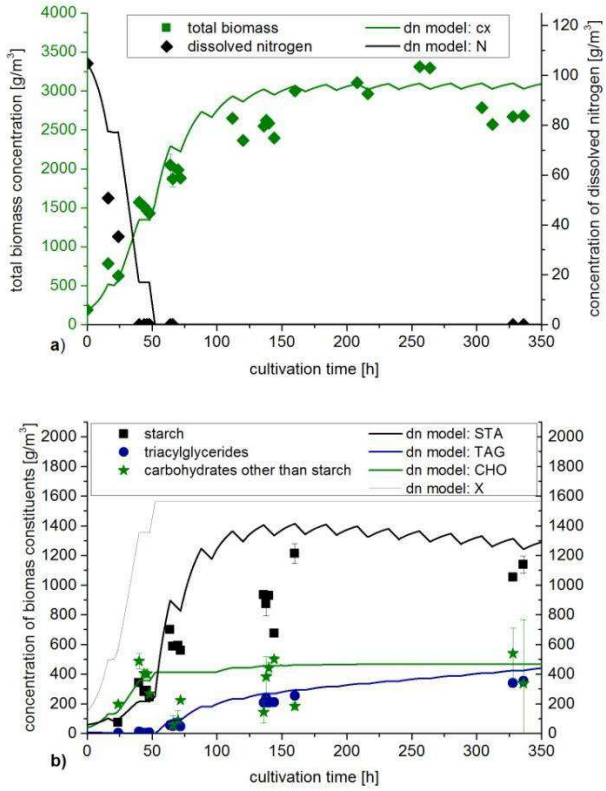

Figure 7: Model simulation of the day night cycle experiment. Solid lines represent the model output and symbols represent the experimentally obtained data. Concentrations of the total biomass (cx, green squares, green line) and nitrogen (N(-NO_3^-), black diamonds, black line) are shown in (a). The concentrations of the measurable amount of starch (STAm, black squares, black line) and carbohydrates other than starch (CHOm, green stars, green line) as well as the concentration of triacylglycerides (TAG, blue circles, blue line) and the simulated concentration of reproducing biomass (X, grey line) are presented in (b). All data points are the average of two technical replicates. In some cases, the error bars representing single measurements are covered by a symbol.

In the model, a constant maintenance requirement of reproducing biomass is assumed to be the only effect causing dark respiration. Nevertheless, dark respiration varies dependent on the temperature [38], duration of darkness, irradiance and temperature before darkness [43] and the cells' physiological state in their life cycle [44]. Under extreme conditions, e.g. salinity, high light and nutrient depletion, the entire biomass produced in daylight is respired during the night to supply energy for maintenance [45]. Understanding the biological mechanisms that influence the maintenance requirement would allow an accurate description of dark respiration. The incorporation of a 'stress factor' into the model representing the increase of the maintenance requirement due to stress conditions may deliver a sufficient approach to estimate the maintenance requirement in metabolic models. The 'stress factors' should be based on experimental testing of the separate influences.

Additionally to the maintenance requirement, other energy requirements occur under nitrogen replete conditions. The biomass specific dark respiration was reported to be increasing with nitrate assimilation due to protein synthesis during nights [46, 47]. In several marine and freshwater algae species, carbohydrates and other metabolites were incorporated into proteins during the night leading to protein synthesis rates at night that even equaled the rates in daylight [47]. The additional energy requirement for synthesis of proteins justifies the decrease of other carbohydrates than starch under nitrogen replete conditions, if the amount of starch is not sufficient to supply the energy demand.

The starch content increased more during daytime than it could have been increasing due to the starch fraction in reproducing biomass. Therefore, a starch replacing mechanism for nitrogen replete conditions was incorporated into the model. The mechanism needs to be investigated further with data of the biomass composition during daytime under nitrogen replete conditions.

In summary, the trends of biomass constituent and nitrate concentrations could roughly be simulated during the day night cycles. The model could be improved by the experimental determination of the maintenance requirement dependent on cultivation conditions. Further on, mechanisms of protein and pigment production during the night and replacing mechanisms of the converted and degraded biomass constituents need to be explored under nitrogen replete conditions.

4.5 Local sensitivity analysis

The sensitivities of all parameters and the initial concentrations of the continuous light cultivation were locally analyzed. Compared to the baseline scenario, the inputs were varied by ±10%. The outputs of the sensitivity analysis were the productivities of the total biomass and TAG. For continuous light the productivities after 200.0 h and for day night cycles the productivities after 306.7 h were investigated. These time points were chosen since the productivities are then based on the same light input. The parameters that showed the highest sensitivity in continuous light (Figure 8), were also investigated in the day night cycles (Figure 9).

The predicted productivities of the total biomass and TAG were 0.369 g DW/L/d and 0.044 g TAG/L/d in continuous light. The major effect on the total biomass concentration was caused by the minimum cellular nitrogen content (Qmin) and the initial nitrate concentration (N0). A decrease in the minimum nitrogen content allows more biomass accumulation, if the same amount of nitrogen is supplied. Simultaneously, the cellular nitrogen content drops below the value at which conversion of starch to TAG is induced and, thus, the TAG productivity is increased. At higher initial dissolved nitrate concentration the amount of generated reproducing biomass is increased leading to a proportional increase of the total biomass and TAG productivity. The TAG productivity is most sensitive to carbon partitioning, which is described using pA and pB, whereas only a slight effect on the total biomass concentration is observed for the variations in these parameters.

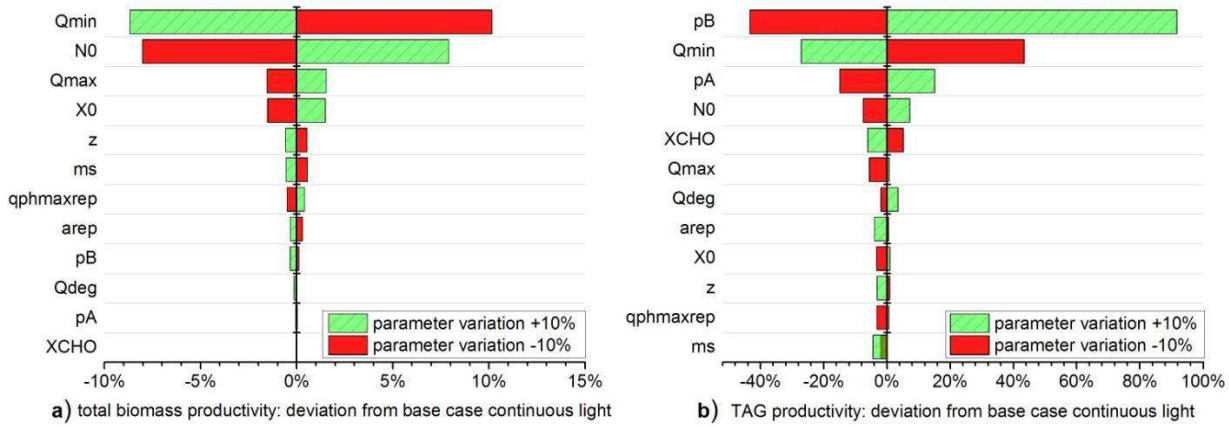

Figure 8: Local sensitivity analyzes of the continuous light simulation. Parameters were altered ±10% compared to the base case scenario. The deviation of the total biomass productivity (a, base case: 0.369 g DW/L/d) and the TAG productivity (b, base case: 0.044 g TAG/L/d) relative to the productivities predicted by the base case scenario is shown for t=200.0 h. Note: (a) and (b) are scaled differently. Green bar represent the positive and red bars the negative deviation of the input. With pA and pB: parameter defining the correlation of the partition coefficient f_{TAG} to the cellular nitrogen content, Qmin: minimum cellular nitrogen content, Qmax: nitrogen content of nitrogen repleted biomass, z: light path of the reactor, XCHO: fraction of carbohydrates other than starch in the total biomass and ms: maintenance requirement, N0 and X0: initial concentrations of dissolved nitrogen ($N\text{-}NO_3^-$) and reproducing biomass, qphmaxrep: maximum photosynthetic rate, arep: absorption cross section under nitrogen replete conditions, Qdeg: cellular nitrogen content below which starch is converted to TAG.

The predicted biomass productivity in day night cycles (0.240 g DW/L/d) was 1.5 times lower and the TAG productivity (0.032 g TAG/L/d) 1.4 times lower compared to continuous light after the same light input. The cultivation time in continuous light was approximately 1.5 times lower than in day night cycles. Thus, the yields on photons predicted by the model are similar. Predominantly, this is a consequence of the estimated parameters pA and pB that define carbon partitioning between TAG and starch. The sensitivity of pB was higher in day night cycles compared to the sensitivity of other altered parameters. The high sensitivity of pA and pB demonstrates that these parameters need to be precisely defined to achieve reliable predictions. The effect is caused by the higher energy content in TAG compared to starch, which leads to a decrease of biomass accumulation at higher TAG production rates [3].

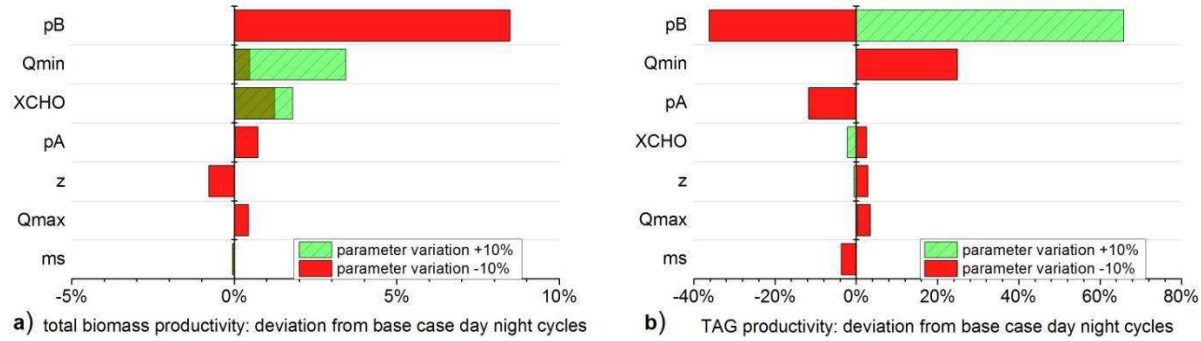

Figure 9: Local sensitivity analyzes of the day night cycle simulation. Parameters were altered ±10% compared to the base case scenario. The deviation of the total biomass productivity (a, base case: 0.240 g DW/L/d) and the TAG productivity (b, base case: 0.032 g TAG/L/d) relative to the productivities predicted by the base case scenario is shown for t=306.7 h. Note: (a) and (b) are scaled differently. Green bar represent the positive and red bars the negative deviation of the input. Only the negative deviation of the inputs pA, Qmin and ms were simulated due to time limitations. With pA and pB: parameter defining the correlation of the partition coefficient f_{TAG} to the cellular nitrogen content, Qmin: minimum cellular nitrogen content, Qmax: nitrogen content after the first night of nitrogen depletion, z: light path of the reactor, XCHO: fraction of carbohydrates other than starch in the total biomass and ms: maintenance requirement.

5 Perspectives

A nitrogen run-out cultivation with *Chlorococcum littorale* was performed under continuous light conditions to estimate the strain specific model parameters. The model was calibrated by fitting the maintenance requirement resulting in accurate simulations of the concentrations of the total biomass, the reproducing biomass, triacylglycerides (TAG) and starch under nitrogen deplete conditions. No further adjustments in the model were required. Under nitrogen replete conditions, the biomass specific growth rate was underestimated, which is likely to be avoided by a higher frequency of dry weight analysis to obtain the actual maximum growth rate. For the model validation with *C. littorale* at least one biological replicate is required, since only one experiment with this set up was performed. In inoculum preparation, more focus should be placed on nitrogen replete conditions to exclude a potential effect of the extent of nitrogen depletion on the growth rate after inoculation.

A second experiment was performed analogous to the one described before, but included a day night cycle (16:8 h). The yields of biomass on photons were equal in both experiments, even though biomass was degraded during the nights, mainly as starch. Nevertheless, the biomass concentrations differed due to higher TAG accumulation in continuous light when compared to day night cycles based on the same energy input. A comparison of the photosynthetic efficiencies in continuous light and day night cycles is impossible based on the obtained data due to the following reasons: The measured compositions did not allow a reliable estimation of the energy content of the biomass and the total amount of the respired biomass is uncertain, since only three nights were analyzed. Furthermore, a difference in the reproducing biomass composition (i.e. the energy content), in continuous light and day night cycles is assumed due to the lower estimated cellular nitrogen content

occurring with a higher absorption cross section. For a reliable comparison of the photosynthetic efficiencies in terms of biomass production, the concentrations of biomass constituents need to be measured at least at the beginning and the end of all nights in a sequential period of the cultivation time.

The first step of adjusting the model to day night cycles was implementing the light change. The only clear trend observed in all investigated nights was the degradation of starch. Thus, starch degradation was incorporated into the model to supply the energy for maintenance during the nights. The maintenance requirement was estimated by fitting in the continuous light model and does not necessarily represent its biological meaning. The experimental determination of the maintenance requirement under different conditions (e.g. the extent of nitrogen depletion, duration of light hours, temperature and light intensity) would represent its biological meaning and, therefore, justifies the maintenance requirement as the basis for the mechanism of dark respiration. By itself, this mechanism does not represent the entire experimentally observed biomass degradation. The additional biomass degradation under nitrogen replete conditions is assumed to be caused by the synthesis of nitrogen containing constituents on the expense of (mainly) carbohydrates. These carbohydrates were considered to be restored during daytime, but experimental validation is required. Further on, the concentrations of the most abundant nitrogen containing biomass constituents (proteins, pigments, RNA, DNA and membrane lipids) need to be investigated to estimate their production rates in the day night cycles under nitrogen replete conditions. The carbon partitioning module needs to be enhanced with one constituent that summarizes all nitrogen containing compounds, if the rates are equal or with several constituents, if the rates differ. The latter approach results in a more detailed description of the potential biorefinery feedstock.

In conclusion, for the validation of the model in continuous light, at least one biological replicate and the analysis of the statistical significance of the predicted biomass constituent concentrations are required. The model of day night cycles needs to be extended to describe carbon partitioning during nights and the effect of nights on the production of biomass constituents during daytime.

After the complete adjustment of the model of day night cycles based on the recommended experiments, several steps need to be taken to achieve a prediction of outdoor conditions. These include the temperature and light distribution [14, 18, 19] as external conditions and their influence on the local production rates [15]. Effects of stress conditions, such as extreme temperatures and high light, need to be experimentally determined and incorporated for the applicability under changing environmental conditions.

6 Appendix

6.1 Model description for continuous light cultivations

Carbon partitioning between different biomass constituents is described in 6.1.2. A set of ordinary differential equations ((Eq. 13)-(Eq. 17)) describes production rates of biomass constituents for a batch cultivation.

$$\frac{dX}{dt} = qX \cdot c_x \quad \text{(Eq. 13)}$$

$$\frac{dTAG}{dt} = qTAG \cdot c_x \quad \text{(Eq. 14)}$$

$$\frac{dSTA}{dt} = qSTA \cdot c_x \quad \text{(Eq. 15)}$$

$$\frac{dCHO}{dt} = qCHO \cdot c_x \quad \text{(Eq. 16)}$$

$$\frac{dN}{dt} = qN \cdot c_x \quad \text{(Eq. 17)}$$

$$c_x = X + TAG + STA + CHO \quad \text{(Eq. 18)}$$

Concentrations of reproducing biomass (Eq. 13), TAG (Eq. 14), STA (Eq. 15); CHO (Eq. 16) and dissolved nitrogen (Eq. 17) are generated as a function of time by solving these equations. The biomass specific production rates for each biomass constituent (qX, qTAG, qSTA, qCHO) depend on the available photosynthetic energy, existing biomass composition, extent of nitrogen starvation, and availability of dissolved nitrogen as described in 0. The total biomass concentration (c_x) is the sum of the reproducing biomass (X) and the biomass constituents TAG, STA, and CHO (Eq. 18). Other constituents (e.g. ash) are neglected.

6.1.1 Available energy from photosynthesis

The available photosynthetic energy depends on metabolic regulation and physiological effects, which are influenced by the stage of nitrogen starvation. This progress is described using the cellular nitrogen content (Eq. 19) as a proxy.

$$Q = Q_{max} \cdot \frac{X}{c_x} \quad \text{(Eq. 19)}$$

The composition of reproducing biomass, thus, also its fraction of nitrogen (Q), is assumed to be constant at the maximum cellular nitrogen content (Q_{max}). Since all other biomass constituents do

not contain nitrogen, the cellular nitrogen content is proportional to the fraction of reproducing biomass in the total biomass.

The maximum photosynthetic rate ($q_{ph,max}$, (Eq. 20)) specifies the maximum amount of photons absorbed per dry weight of biomass and time.

$$q_{ph,max} = q_{ph,max,rep} \cdot \frac{(Q - Q_{min})}{(Q_{max} - Q_{min})} \quad \text{(Eq. 20)}$$

A linear decrease of the maximum photosynthetic rate with the cellular nitrogen content (Q) is described by. The maximum is reached at nitrogen replete conditions ($q_{ph,max,rep}$) and zero at the minimum cellular nitrogen content (Q_{min}).

Assuming a homogeneous culture, the average biomass specific photosynthetic rate ($q_{ph,avg}$) in a flat panel photobioreactor with unilateral light supply (Eq. 21) is defined as the average of the integrated photosynthetic rate over the light path (z).

$$q_{ph,avg} = \frac{1}{z} \int_0^z q_{ph,max} \cdot \tanh\left(\frac{a \cdot QY \cdot I_0 \cdot e^{-a \cdot c_x \cdot z}}{q_{ph,max}}\right) \quad \text{(Eq. 21)}$$

The photosynthesis-irradiance response curve with the hyperbolic tangent function gives the photosynthetic rate as a function of light intensity. The attenuation model of Lambert-Beer (Eq. 22) is used to describe the light conditions throughout the reactor.

$$I(z) = I_0 \cdot e^{-a \cdot c_x \cdot z} \quad \text{(Eq. 22)}$$

The ingoing light with the incident light intensity I_0 is passing perpendicularly into the reactor and all scattering is neglected. Therefore, the local light intensity is solely dependent on the attenuation coefficient (a), the total biomass concentration (c_x) and the position in the reactor along the light path. Based on the assumptions above the attenuation coefficient equals the absorption cross section (Eq. 23).

$$a = a_{rep} \cdot \frac{Q}{Q_{max}} \quad \text{(Eq. 23)}$$

The absorption cross section (a) is defined using the absorption cross section under replete conditions (a_{rep}) and Q as a proxy. Pigments are a constant fraction of reproducing biomass and, thus, diluted over the biomass, when other constituents than reproducing biomass are generated.

The photosynthetic quantum yield (QY (Eq. 24)) represents the fraction of absorbed photons that is available for maintenance and synthesis of metabolites.

$$QY = \left(1 - \frac{Q_{min}}{Q}\right) \cdot \left(1 - \frac{Q_{min}}{Q_{max}}\right)^{-1} \quad \text{(Eq. 24)}$$

The remaining fraction (1-QY) is dissipated as heat. In the Droop equation QY is kept between zero and one by the second term, while one occurs at nitrogen replete conditions and zero at the minimum nitrogen content.

6.1.2 Carbon partitioning

Estimations of biomass specific production rates are required to determine the concentrations of biomass constituents based on the average biomass specific photosynthetic rate. The available energy is partitioned to the *de novo* synthesis of biomass constituents with respect to differing yields for TAG, STA, CHO and reproducing biomass estimated, which have been analyzed through flux balance analyzes. Additionally, the following inter-conversions occur. Breuer *et al.* described the conversion of STA to TAG. As a model extension, yields and reaction rates for the conversion of STA and TAG to reproducing biomass were included allowing non-reproducing biomass being present as initial model input. The direction of synthesis and conversion are indicated in Figure 5.

The energy required for the biomass specific maintenance rate is depends only on the cellular nitrogen content (Q), or in other words, the fraction of reproducing biomass.

The dissolved nitrogen concentration (N) is regarded as the trigger between nitrogen replete and nitrogen deplete conditions. If dissolved nitrogen (as nitrate) is available, nitrogen can be incorporated into biomass, so, only reproducing biomass is built (Eq. 25) with a certain yield on photons (yXph).

$$qX = \begin{cases} \overbrace{yXph \cdot \left(q_{ph,avg} - \frac{m_s \cdot Q}{Q_{max}}\right)}^{qX1} + r_{STA/X} \cdot yXSTA + r_{TAG/X} \cdot yXTAG & \text{if } N > 0 \\ 0 & \text{if } N = 0 \end{cases} \quad \text{(Eq. 25)}$$

$$qN = -qX \cdot Q_{max} \quad \text{(Eq. 26)}$$

The biomass specific production rate of reproducing biomass is extended with two terms describing the conversion of STA and TAG to reproducing biomass, respectively. Therefore, the rate of degradation ($r_{STA/X}$ (Eq. 34) and $r_{TAG/X}$ (Eq. 35)) is multiplied with the yield of reproducing biomass on STA (yXSTA) and TAG (yXTAG), respectively. Without dissolved nitrogen, no reproducing biomass can be synthesized. Thus, the biomass specific nitrogen consumption rate (Eq. 26) is only dependent on qX.

Under nitrogen deplete conditions, the production of CHO, STA and TAG occur simultaneously according to different mechanisms. The highest priority is set on CHO production (Eq. 27).

$$qCHO = \begin{cases} \left(q_{ph,avg} - \frac{m_s \cdot Q}{Q_{max}} - \frac{qX1}{yXph}\right) \cdot yCHOph & \text{if } \frac{XCHOX \cdot X + CHO}{c_x} \leq XCHO \\ 0 & \text{if } \frac{XCHOX \cdot X + CHO}{c_x} > XCHO \end{cases} \quad \text{(Eq. 27)}$$

In case, the fraction of CHO in the total biomass is lower than a certain value (XCHO), CHO is produced. The fraction in the total biomass includes the fraction in reproducing biomass (XCHOX) and CHO. The biomass specific CHO production rate is the product of the available energy and the production yield of CHO on photons (yCHOph).

The remaining energy after CHO production is directed to the synthesis of TAG and STA. The partitioning of TAG and STA production is determined by the progress of nitrogen starvation ((Eq. 28) and (Eq. 29)).

$$qTAG = \left\{ \left(q_{ph,avg} - \frac{m_s \cdot Q}{Q_{max}} - \frac{qX1}{yXph} - \frac{qCHO}{yCHOph}\right) \cdot f_{TAG} \cdot yTAGph + r_{STA/TAG} \cdot yTAGSTA - r_{TAG/X} \right\} \quad \text{(Eq. 30)}$$

$$qSTA = \left\{ \left(q_{ph,avg} - \frac{m_s \cdot Q}{Q_{max}} - \frac{qX1}{yXph} - \frac{qCHO}{yCHOph}\right) \cdot (1 - f_{TAG}) \cdot ySTAph - r_{STA/TAG} - r_{STA/X} \right\} \quad \text{(Eq. 31)}$$

An experimentally observed factor (f_{TAG}) has been incorporated. This factor defines the energy fraction that is used for TAG production (Eq. 37) as a function of the cellular nitrogen content. The remaining energy fraction drives the production of STA (1-f_{TAG}). Thus, the biomass specific production rate of TAG and STA only based on photosynthetic energy is represented by the first line of (Eq. 30) and (Eq. 31) with the yields yTAGph and ySTAph on photons, respectively. Additionally, STA is converted to TAG at a constant rate ($r_{STA/TAG}$ (Eq. 33)) during the later progress of nitrogen starvation. Taking into account the yield of TAG on STA (yTAGSTA (w/w)) the TAG production rate is increased, while the total biomass production rate is decreased by this mechanism. The model is extended with conversion rates of TAG and STA to reproducing biomass ($r_{TAG/X}$ and $r_{STA/X}$, respectively).

For the conversion of STA to TAG (Eq. 32)(Eq. 37) and STA and TAG to reproducing biomass ((Eq. 34) and (Eq. 35)) 0th order kinetics are assumed.

$$r_{STA/TAG} = \begin{cases} r_{STA/TAG,max} & \text{if } Q \leq Q_{deg} \text{ and } STA > 0 \\ 0 & \text{if } Q > Q_{deg} \text{ and } STA = 0 \end{cases} \quad \text{(Eq. 33)}$$

$$r_{STA/X} = \begin{cases} r_{STA/X,max} & \text{if } N > 0 \text{ and } STA > 0 \\ 0 & \text{if } N < 0 \text{ or } STA = 0 \end{cases} \quad \text{(Eq. 34)}$$

$$r_{TAG/X} = \begin{cases} r_{TAG/X,max} & \text{if } N > 0 \text{ and } TAG > 0 \\ 0 & \text{if } N < 0 \text{ or } TAG = 0 \end{cases} \quad \text{(Eq. 35)}$$

Conversion processes can only occur, if the reagent is present, so the concentration is above zero. Further on, STA degradation was found to occur only below the cellular nitrogen content Q_{deg}. Dissolved nitrogen is required to be incorporated into reproducing biomass, so conversion of STA and TAG to reproducing cannot occur under nitrogen deplete conditions.

6.2 Parameter estimation: methods and biological background

6.2.1 Theoretical parameters

The maximum production yields of biomass constituents on photons (yXph, yCHOph, ySTAph and yTAGph) as well as the conversion yield of TAG on starch (yTAGSTA) were obtained based on flux balances analyzes by Kliphuis *et al.* [23]. Additionally, the conversion yields of reproducing biomass on TAG (yXTAG) and starch (yXSTA), the yield of ATP on photons (yATPph) and the yield of ATP on starch (yATPSTA) were estimated based on metabolic pathways as described in 6.2.4.

6.2.2 Experimentally derived parameters

The following parameters were derived similar to the initial parameter estimation performed by Breuer *et al.* [27]: maximum biomass specific photosynthetic rate under replete conditions ($q_{ph,max,rep}$); minimum nitrogen content (Q_{min}); nitrogen content, below which starch was converted to TAG (Q_{deg}); maximum inter-conversion rate of starch to TAG ($r_{STA/TAG,max}$); pA and pB.

The parameters pA and pB are coefficients correlating the partition coefficient f_{TAG} (Eq. 36) to the cellular nitrogen content (Q) following an exponential equation (Eq. 37).

$$f_{TAG} = \frac{\text{photons for TAG synthesis}}{\text{photons for starch synthesis}} = \frac{\Delta TAG}{\Delta TAG + \frac{\Delta STA \cdot yTAGph}{ySTAph}} \quad \text{(Eq. 36)}$$

The partition coefficient f_{TAG} is defined as the ratio of the amount of photons used for the production of TAG to the amount of photons used for the production of TAG and STA. For the parameter estimation, the amount of generated STA (ΔSTA) is transformed to the amount of TAG, that could have been produced instead, using the yields of STA and TAG on photons (ySTAph and yTAGph).

$$f_{TAG} = \min \begin{Bmatrix} pA \cdot Q^{-pB} \\ 1 \end{Bmatrix} \quad \text{(Eq. 37)}$$

(Eq. 37) describes carbon partitioning between STA and TAG using the cellular nitrogen content (Q) as a proxy to define it at any time point of the cultivation. The empirical approach is used, since the metabolic regulation is not sufficiently understood to be mechanistically modeled. The parameters pA and pB for continuous light and day night cycles differed (Table 1).

The maximum photosynthetic rates also differed for continuous light and day night cycles. The maximum inter-conversion rate of TAG and starch to reproducing biomass ($r_{TAG/X,max}$ and $r_{STA/X,max}$) and the composition of reproducing biomass (XSTAX and XCHOX) were estimated based on the continuous light experiment and assumed to hold for day night cycles. The maximum cellular nitrogen content (Q_{max}) was redefined as the nitrogen content associated with the highest biomass specific absorption cross section between 400 and 700 nm (Eq. 38).

$$a_{rep} = \frac{\sum_{400}^{700} abs_{\lambda} \frac{\ln(10)}{z}}{301 \cdot c_{DW}} \quad \text{(Eq. 38)}$$

with z: light path of the precision cell
c_{DW}: dry weight concentration in the cell

The absorption (abs_{λ}) was corrected for scattering by subtracting the average absorption between 740 and 750 nm.

The fraction of carbohydrates other than starch (XCHO) after nitrogen depletion, the initial TAG and dissolved nitrogen concentration were directly obtained from experimental data (4.1). The initial concentrations of STA and CHO were estimated from the measurable concentrations (STAm (Eq. 39) and CHOm (Eq. 40)).

$$STAm = (X \cdot XSTAX - degSTA + STA) \quad \text{(Eq. 39)}$$

$$CHOm = ((X + degSTA) \cdot XCHOX + CHO) \quad \text{(Eq. 40)}$$

For this estimation the contents of starch (XSTAX) and carbohydrates other than starch (XCHOX) in reproducing biomass as well as the amount of starch degraded from reproducing biomass (degSTA) were taken into account.

All parameters described in this chapter (6.2.2) were directly used in the model without any fitting (see supplementary data for more details).

6.2.3 Fitted parameters

The maintenance requirement (m_s) was estimated by minimizing the normalized sum of squared differences, so maximizing R-square (Eq. 41), of the biomass concentration throughout the

continuous light cultivation. The normalization to the mean was chosen to achieve the same accuracy of the prediction for the entire cultivation time.

$$R^2 = 1 - \frac{SSE}{SST} = 1 - \sum_t \left(\frac{c_x(t) - \mathrm{model}c_x(t)}{c_x(t) - cx_{avg}} \right)^2 \quad \text{(Eq. 41)}$$

The estimated maintenance requirement of $6.24 \cdot 10^{-7}$ mol photon/g X/s (supplementary data) used in day night cycles to quantify the energy demand during night causing dark respiration.

The partition coefficient for restoring the respired amount of starch (f_{part}) was estimated using the same approach. The sum of R-squares of the total biomass concentration, the starch concentration and the TAG concentration was maximized to estimate the most realistic value for the partition coefficient f_{part}. Since no distinct maximum of the sum of R-squares could be observed, the R-squares of all concentrations (cx, X, CHOm, STAm, TAG and N) were manually evaluated to estimate an appropriate range for f_{part}. All R-squares showed the highest values in the range of 0.0 to 0.2 and 0.50 to 0.57, while the fit quality was decreasing at $f_{part}>0.2$. Both ranges were therefore further evaluated resulting in $f_{part}=0.03$ (supplementary data).

Table 2: Parameters with constant values for cultivation under continuous light conditions and day night cycles.

parameter	value	unit	definition
maximum photosynthetic yields based on flux model analysis of *C. reinhardtii* [23]			
yXph	1.62	$\frac{\text{g X}}{\text{mol photon}}$	yield of reproducing biomass on photons
yCHOph	3.24	$\frac{\text{g CHO}}{\text{mol photon}}$	yield of other carbohydrates than starch on photons
ySTAph	3.24	$\frac{\text{g STA}}{\text{mol photon}}$	yield of starch on photons
yTAGph	1.33	$\frac{\text{g TAG}}{\text{mol photon}}$	yield of triacylglycerides on photons
yTAGSTA	0.39	$\frac{\text{g TAG}}{\text{g STA}}$	conversion yield of triacylglycerides on starch
theoretical yields based on metabolic pathways described in 6.2.1			
yXSTA	0.64	$\frac{\text{g X}}{\text{g STA}}$	conversion yield of reproducing biomass on starch
yXTAG	1.40	$\frac{\text{g X}}{\text{g TAG}}$	conversion yield of reproducing biomass on triacylglycerides
yATPph	0.38	$\frac{\text{mol ATP}}{\text{mol photon}}$	yield of ATP on photons
yATPSTA	0.15	$\frac{\text{mol ATP}}{\text{g STA}}$	yield of ATP on starch
experimentally estimated parameters of continuous light cultivation			
XCHOX	26.27%	$\frac{\text{g CHO}}{\text{g DW}}$	carbohydrate other than starch fraction in reproducing biomass
XSTAX	16.56%	$\frac{\text{g STA}}{\text{g DW}}$	starch fraction in reproducing biomass
Q_{min}	3.65%	$\frac{\text{g N}}{\text{g DW}}$	minimum cellular nitrogen content
Q_{deg}	3.65%	$\frac{\text{g N}}{\text{g DW}}$	nitrogen content below starch is converted to TAG
$r_{STA/TAG,(max)}$	$1.87 \cdot 10^{-8}$	$\frac{\text{g STA}}{\text{g DW} \cdot \text{s}}$	(maximum) conversion rate of starch to triacylglycerides, $r_{\text{STA/ TAG,max}} = \frac{\text{XSTA}_{t1} - \text{XSTA}_{t2}}{t_2 - t_1}$
$r_{TAG/X,(max)}$	$2.03 \cdot 10^{-7}$	$\frac{\text{g TAG}}{\text{g DW} \cdot \text{s}}$	(maximum) conversion rate of triacylglycerides to reproducing biomass, $r_{\text{TAG/ X,max}} = \frac{\text{XTAG}_{t1} - \text{XTAG}_{t2}}{t_2 - t_1}$
$r_{STA/X,(max)}$	$8.05 \cdot 10^{-7}$	$\frac{\text{g STA}}{\text{g DW} \cdot \text{s}}$	(maximum) conversion rate of starch to reproducing biomass, $r_{\text{STA/ X,max}} = \frac{\text{XSTA}_{t1} - \text{XSTA}_{t2}}{t_2 - t_1}$
m_s	$6.25 \cdot 10^{-7}$	$\frac{\text{mol photon}}{\text{g DW} \cdot \frac{Q}{Q_{max}} \cdot \text{s}}$	maintenance requirement per amount of reproducing biomass and time
z	$2.45 \cdot 10^{-2}$	m	light path of the reactor

6.2.4 Biological background: dark respiration

Photosynthetic organisms consume biomass during exposure to darkness or insufficient irradiance. Under these conditions, biomass constituents are oxidized to deliver the energy required for maintenance. This so-called dark respiration has been described through two terms in literature. One

is the ‘biomass specific oxygen uptake rate,’ which is the amount of oxygen consumed per biomass and time. Another term is ‘biomass loss’ describing the respired amount of biomass during a dark period as a ratio to the biomass present before the dark period started. Values for biomass losses range from 2-10% for *Coelastrum sphaericum* and *Scenedesmus falcatus* [44] to 30% in the culture of *Chlorella pyrenoidosa* [40]. Under extreme conditions, the entire biomass produced in daylight is respired during the night [45]. Several factors highly influence dark respiration rates. These include temperature [38], duration of darkness, irradiance and temperature before darkness [43] and the cells’ physiological state in their life cycle [44].

Low respiration rates are crucial for large scale applications to avoid a decrease in biomass productivities. Night biomass losses may be reduced and lipid productivities increased through high temperatures during daytime and low temperatures during nights [40]. Nevertheless, distinguishing between respiration rates of different biomass constituents is important to select appropriate conditions and strains for synthesizing a certain product.

Under stress conditions, starch and triacylglycerides (TAGs) are the most abundant carbon and energy storage components in many microalgae such as *Chlorococcum littorale* [48, 49]. These storage components are converted to reproducing biomass under nitrogen replete conditions. During nights preferentially storage components are respired to supply energy for maintenance processes. Yields of adenosine triphosphate (ATP) equivalents on each constituent are calculated based on simplified metabolic pathways, which are used to describe conversion and degradation in the model (for a detailed description see 6.2.4.1 to 6.2.4.4). The net reactions of all pathways considered are summarized in Table 3, namely, the upper and lower glycolysis, oxidative pentose-phosphate pathway, glycerin degradation, fatty acid activation, β-oxidation, tricarboxylic acid (TCA) cycle and reactions in different complexes of oxidative phosphorylation.

Table 3: Balances of metabolites (input and output) and energy carriers (profit and costs) are shown for a certain pathway of carbohydrate and TAG degradation. Abbreviations are defined in Table 5 (p. Fehler! Textmarke nicht definiert.**).**

Pathway	Source	Input	Output	Profit	Costs
Upper glycolysis	7/8th glucose from starch	1 G6P	2 G3P	-	2 ATP*
OPPP	1/8th glucose from starch	1 G6P	-	12 NADPH	1 ATP*
Lower glycolysis	upper glycolysis, glycerin degradation	1 G3P	1 acetyl-CoA	2 NADH** 2 ATP	-
Glycerin degradation	TAG	1 glycerin	G3P	1 NADH	1 ATP
FA activation	TAG	3 FA (C18)	3 acyl-CoA	-	3 ATP
β-oxidation	fatty acid activation	3 acyl-CoA	27 acetyl-CoA	24 NADH 24 $FADH_2$	-
TCA cycle	lower glycolysis, β-oxidation	1 acetyl-CoA	-	3 NADH 1 $FADH_2$ 1 GTP	-
oxidative phosphorylation					
		$H^+_{translocated\ from\ matrix\ to\ intermembrane\ space}$		**Profit**	**Costs**
NADH-Q oxidoreductase (I)		4		QH_2	1 NADH
Succinate-Q oxidoreductase (II)		-		QH_2	1 $FADH_2$
Q-cyt c oxidoreductase (III)		6		3 cyt c	2 QH_2
Cyt c-oxidase (IV)		1		-	1 cyt c 1 H^+_{matrix}
ATP synthase		–13		3 ATP	3 ADP, 3 P
Phosphate transfer from intermembrane space to matrix		–1			

*including 1 ATP for conversion of glucose to G6P

**including 1 NADH from conversion of pyruvate to acetyl group

The degradation of starch and TAG results in the yields 0.149 mol ATP/g starch and 0.325 mol ATP/g TAG. The difference between these yields is caused by the higher energy content of TAG per carbon atom [39] and by the higher fraction of carbon atoms in TAG. As a simplification, conversion yields from other biomass constituents to reproducing biomass are based on total breakdown and *de novo* synthesis causing an overestimation of ATP requirement.

The maximum yield of reproducing biomass on photons was determined to be 1.62 g/mol photon in *C. reinhardtii* [27]. Generation of three ATP is driven by eight absorbed photons [23] resulting in a yield of 4.320 g reproducing biomass/mol ATP. The conversion yields result in 0.644 g reproducing biomass/starch or other carbohydrates and 1.404 g reproducing biomass/g TAG. In conclusion, while the conversion of starch to reproducing biomass leads to unavoidable biomass losses, the conversion of TAG to reproducing biomass may result in an increase of the amount of biomass without net carbon fixation. The pathways of carbohydrate and TAG breakdown to ATP equivalents are described below (6.2.4.1 to 6.2.8). The resulting yields of conversion to reproducing biomass and ATP are summarized in Table 3 of the main report.

6.2.4.1 Respiration of starch and other carbohydrates

Many microalgae strains accumulate starch granules when cell division is prohibited, e.g. by insufficient nitrogen supply [50]. In contrast, other carbohydrates than starch - mainly pectin, agar, alginate and cellulose - are present in the cell wall [36] and their concentration is constant under nitrogen starvation [27]. Other carbohydrates than starch are assumed to be converted to energy carriers with the same ATP yields as starch. The metabolic pathway (Figure 10) is based on studies of the model organism *Chlamydomonas reinhardtii* [39] and is assumed to be similar to the one of *C. littorale* since both are green algae. Few studies have been performed on *C. littorale*, so a description of its specific metabolic pathways is not available.

In absence of light and carbon sources starch is broken down through glycolysis or the oxidative pentose-phosphate pathway (OPPP), alternatively (Figure 10) [39]. As the initial step of respiration, starch is expected to be converted to glucose, for instance, catalyzed by amylase in the chloroplast stroma [50]. No specific energy consumption is assumed for depolymerization. Following, glucose is phosphorylated to glucose 6-phosphate (G6P) by hexokinase dephosphorylating one ATP molecule. Further on, $7/8^{th}$ of G6P is assumed to be broken down through glycolysis, while $1/8^{th}$ takes the OPPP on average [39].

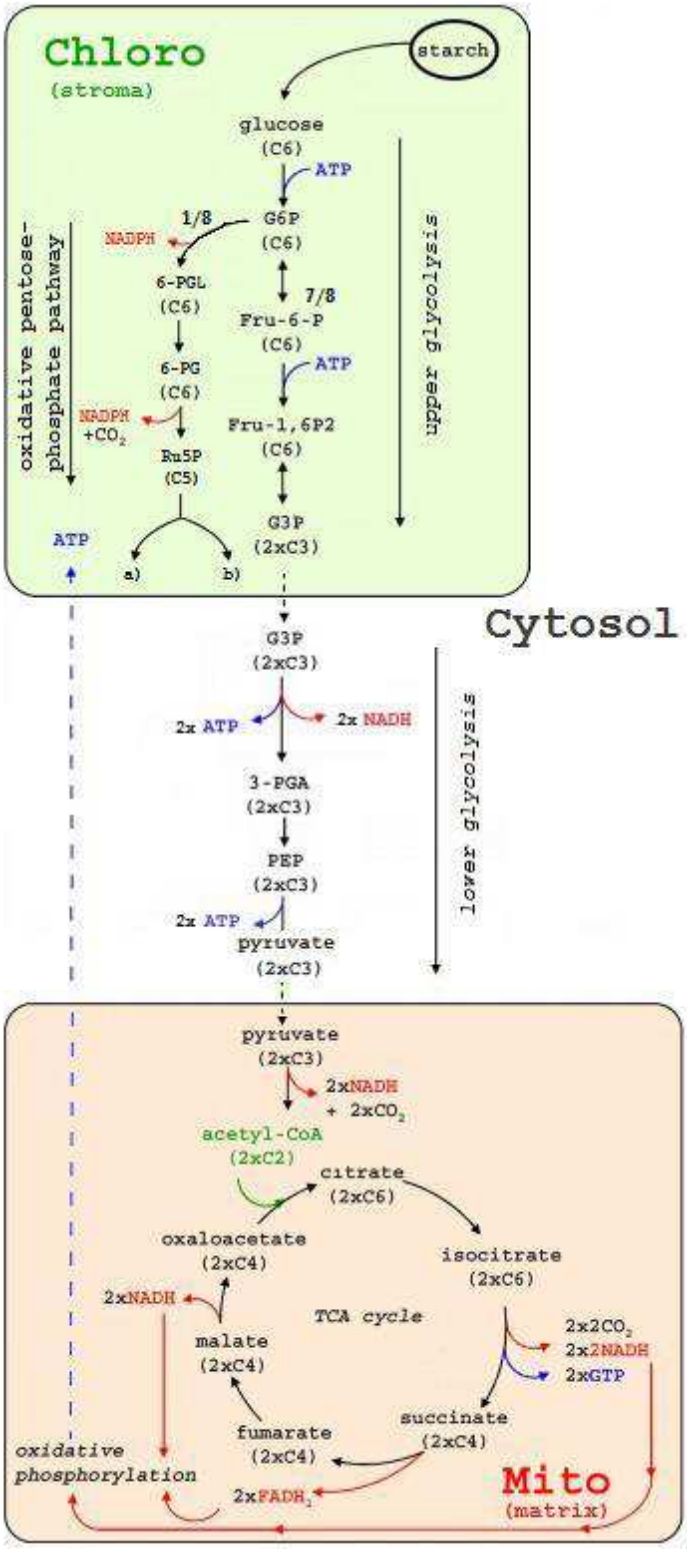

Figure 10: Simplified starch degradation. The starch breakdown includes depolymerization of starch and oxidation through the glycolysis and the oxidative pentose-phosphate pathway as well as the TCA cycle. ATP is generated from all energy carriers built by the oxidative phosphorylation. A list of all abbreviations is given in Table 5. For a more detailed description see 6.2.4.3, 6.2.4.4 and 6.2.7. Simplified and adapted from [39].

6.2.4.2 Upper glycolysis

The upper glycolysis continues, converting G6P to fructose-6-phosphate (Fru-6-P) catalyzed by phosphoglucose isomerase. Subsequently, Fru-6-P is phosphorylated to fructose 1,6-bisphosphate (Fru-1,6P2) using one ATP. The last step of the upper glycolysis is the conversion into two glyceraldehyde-3-phosphate (G3P) resulting in net costs of two ATP per glucose molecule. G3P is transported from the chloroplast stroma to the cytosol through the outer chloroplast membrane by a triose-phosphate translocator [39], without any energy costs assumed.

6.2.4.3 Oxidative pentose-phosphate pathway

For glucose degradation the OPPP is an alternative pathway to glycolysis. The OPPP is reported to be regulated upon demand for carbon, ATP and the reduced form of nicotinamide adenine dinucleotide phosphate (NADPH) [39]. The reactions may take place in plastids as well as in the cytosol [51]. G6P oxidizes to 6-phosphoglucolactone (6-PGL) by G6P-dehydrogenase reducing one $NADP^+$. 6-PGL is further converted to 6-phosphogluconate (6-PG), which is subsequently decarboxylated to ribulose-5-phosphate (Ru5P) by 6-phosphogluconate dehydrogenase reducing another $NADP^+$ [39, 51]. The oxidative section of this pathway as described above gains 2 NADPH. Nevertheless, for the following reactions different schemes are proposed [51]. Two basic principles of pathways have been observed in *Arabidopsis*, a model organism of higher plants: a) non-oxidative, carbon demanding and b) oxidative, energy demanding pathways. Both principles need to be further evaluated to estimate appropriate yields for conversion of starch and other carbohydrates to other biomass constituents and ATP. The OPPP involves recycling of Fru-6-P and triose phosphate through several enzymatic reactions depending on their dynamic equilibrium [51]. Ru5P is converted to ribose-5-phosphate (R5P), which can be used as a building block (a) [39] to synthesize for instance fatty acids [52] and nucleotides [53]. Alternatively, metabolic intermediates may be regenerated to G6P and path through the OPPP cyclically (b). Only the complete oxidation of metabolic intermediates (pathway b) is evaluated here since energy demand causes dark respiration. All carbon atoms, which are not released as CO_2 are recycled. This results in two NADPH per carbon atom fed to the OPPP or in other words twelve NADPH per glucose [51] minus one ATP for the generation of G6P from glucose.

6.2.4.4 Lower glycolysis

The lack of energy carriers during darkness drives the lower glycolysis. The oxidation of G3P to 1,3-bisphosphoglycerate (1,3-BPG) by glyceraldehyde phosphate dehydrogenase reduces nicotinamide adenine dinucleotide (NAD^+) to NADH [54]. Sequentially, the phosphoglycerate kinase transfers one phosphate group from 1,3-BPG to adenosine diphosphate (ADP) giving 3-phosphoglycerate (3-PGA) and ATP [39]. After the phosphoglycerate mutase has shifted the phosphate group from the third to the second carbon atom, one water molecule is removed by

enolase. In consequence of these reactions, phosphoenolpyruvate (PEP) is built. Pyruvate is formed through transferring the phosphate group from PEP to ADP [55]. Further degradation of pyruvate takes place in the mitochondrial matrix. The outer mitochondrial membrane can be passed through voltage-dependent anion channels [56]. The transfer through the inner mitochondrial membrane is only possible through mitochondrial pyruvate carriers as investigated in yeast but is reported to be highly conserved [57]. Taking no energy costs for transportation into account, the lower glycolysis yields two NADH and four ATP per glucose molecule. Pyruvate is oxidized releasing one carbon dioxide and yielding one NADH. The remaining acetyl group bonds with coenzyme A [58, 59].

6.2.5 Triacylglycerides

TAGs are accumulated in cytosolic lipid bodies under stress conditions, e.g. nitrogen starvation. Depending on the cellular demand, TAGs can be either converted to other metabolites such as polar lipids, or degraded to yield chemical energy [49]. The complete degradation of TAG involves β-oxidation, tricarboxylic acid (TCA) cycle and oxidative phosphorylation (Figure 11) [60].

Prior to β-oxidation free fatty acids are required, which are bound by coenzyme A (CoA) to be degraded through the β-oxidation. TAG is split stepwise into a diacylglyceride or monoacylglyceride by different lipases, before three fatty acids (FA) and one glycerin are released [59].

Different pathways for glycerin degradation have been considered in the literature. Since they result in the same balance of energy carriers, only one is described below. Glycerin is oxidized to glyceraldehyde reducing NAD^+ to NADH. Subsequently, triose kinase phosphorylates glyceraldehyde to G3P using one ATP. G3P enters the lower glycolysis [59].

Each fatty acid reacts each with one ATP to acyl-adenosine monophosphate (AMP) splitting off two inorganic phosphate groups. Afterwards the acyl group is activated by binding CoA at the thio group, while AMP is split off. The resulting acyl-CoA is further degraded through β-oxidation, which takes place in the mitochondrial matrix. The inner mitochondrial membrane is not permeable for acyl-CoA. On the outer mitochondrial membrane, the acyl group is transferred from CoA to carnitine. Acyl-carnitine passes the inner mitochondrial membrane and the acyl group is transferred on another CoA [59]. As the initial step of β-oxidation, acyl-CoA dehydrogenase oxidizes acyl-CoA to trans-enoyl-CoA yielding one reduced flavin adenine dinucleotide ($FADH_2$). The addition of water is catalyzed by enoyl-CoA hydratase and results in β-hydroxyacyl-CoA. The latter is oxidized to β-ketoacyl-CoA by β-hydroxyacyl-CoA dehydrogenase generating one NADH. An additional CoA is bonds with the keto group in β-position, while acetyl-CoA is split off. The remaining acyl-CoA reenters the cycle of β-oxidation until the carbon chain becomes shorter than four atoms [61].

In the current study, all fatty acids in TAG are considered to consist of 18 carbon atoms since they were the most abundant in *Chlorococcum littorale* [31, 41, 62]. Thus, each fatty acid passes eight times through the cycle of β-oxidation. For each TAG molecule, four ATP are used and one NADH as well as one G3P is gained prior to beta-oxidation. The yield of β-oxidation is 24 of each $FADH_2$ and NADH plus 27 acetyl-CoA.

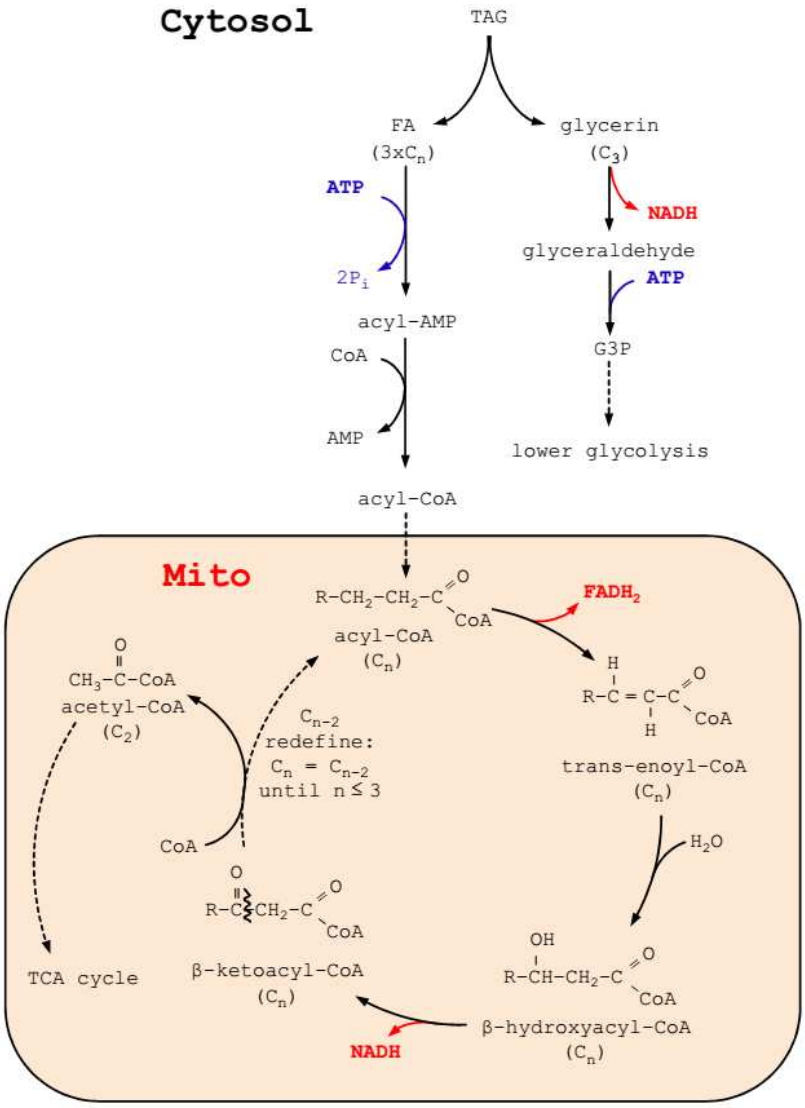

Figure 11: TAG degradation. First, TAG is split into fatty acids and glycerin. Glycerin is further degraded to enter the lower glycolysis, while fatty acids are modified to pass through the β-oxidation. Acetyl-CoA, $FADH_2$ and NADH are gained during β-oxidation, which are directed to the TCA cycle and the oxidative phosphorylation, respectively. A list of all abbreviations is given in Table 5. For a more detailed description see 6.2.4.1, 6.2.6 and 6.2.7.

6.2.6 Tricarboxylic acid cycle

The TCA cycle (Figure 10) is a series of biochemical reactions resulting in the generation of reduced energy carriers NADH, GTP and $FADH_2$. Acetyl-CoA is fed to the TCA cycle. First, citrate is synthesized by transferring the acetyl group on oxaloacetate. After transforming citrate to isocitrate, the oxidation by isocitrate dehydrogenase results in α-ketoglutarate, CO_2 and NADH. The irreversible

oxidative decarboxylation of α-ketoglutarate occurs with a thioester linkage to CoA and the reduction of NAD^+ to NADH catalyzed by α-ketoglutarate dehydrogenase. Succinyl-CoA is built. Breaking of the thioester bond by Succinyl-CoA synthetase releases succinate and CoA as well as energy for phosphorylation of guanosine diphosphate (GDP). The three reactions from isocitrate to succinate are summarized as one net reaction in Figure 10. Subsequently, succinate dehydrogenase oxidizes succinate to fumarate, reducing one FAD. Malate is generated by hydration of fumarate through catalysis of fumarase. As the last step of the TCA cycle, malate is oxidized to oxaloacetate, which reenters the cycle. In this reaction, electrons are transferred to NAD^+ by malate dehydrogenase. The net energy balance of the TCA cycle is three NADH, one GTP and one $FADH_2$ per acetyl-CoA [59, 63].

6.2.7 Oxidative phosphorylation

As a consequence of carbon oxidations in lower glycolysis, TCA cycle and fatty acid degradation, energy carriers are generated (ATP, guanosine triphosphate (GTP), NADH, NADPH and $FADH_2$). In the following, GTP and NADPH are considered as equaling ATP and NADH, respectively, since they are known to be converted from one to the other in several organisms [64, 65]. The oxidative phosphorylation couples carbon oxidation to ATP synthesis through proton translocation utilizing the energy carriers NADH and $FADH_2$ as described below.

The respiratory chain, where oxidative phosphorylation takes place, can be considered to consist of four protein complexes in the inner mitochondrial membrane (Figure 12). These complexes are considered to be randomly dispersed in the membrane and connected by electron shuttles [66]. Three of them (I, III and IV) function as proton pumps from the mitochondrial matrix to the intermembrane space fueled by NADH and $FADH_2$. An additional protein complex, the ATP synthase, uses this proton gradient as a proton motive force to generate ATP [60]. To estimate yields of ATP equivalents on NADH and $FADH_2$, details on the assumed enzymatic processes in the respiratory chain are required.

6.2.7.1 NADH-coenzyme Q oxidoreductase

Complex I, the NADH-Q oxidoreductase, contains flavin mononucleotide (FMN) as the prosthetic group. FMN is reduced to $FMNH_2$ by NADH, which binds to the complex in the mitochondrial matrix. Two electrons are transferred from $FMNH_2$ through several Fe-S-clusters to the coenzyme Q, also named as ubiquinone. Hence, together with two protons from the matrix, coenzyme Q is reduced to ubiquinol (QH_2). Simultaneously, four protons are transferred through the membrane to the intermembrane space [60, 66].

6.2.7.2 Succinate-coenzyme Q oxidoreductase

Complex II also generates QH_2, but oxidizes another substrate. The succinate-dehydrogenase is a subunit of this complex and catalyzes its first reaction as part of the TCA cycle. Succinate is oxidized to fumarate, while FAD is reduced to $FADH_2$. Two protons and two electrons are transferred from $FADH_2$ via Fe-S-clusters to coenzyme Q. No protons are transferred in this complex, therefore, one $FADH_2$ yields one QH_2 in complex II [60, 66].

6.2.7.3 Coenzyme Q-cytochrome c oxidoreductase

QH_2, which is generated in complex I and II, is used for translocation of protons and reduction of cytochrome c (cyt c) in complex III. Coenzyme Q and its reduced form QH_2 are soluble in hydrophobic areas of the inner mitochondrial membrane. Thus, diffusive processes allow the migration between complexes in the respiratory chain. The cofactor cyt c is a water soluble protein, which is released to the intermembrane space and approaches complex IV [60, 66].

Since cyt c is a one-electron acceptor, only one electron can be taken up from each QH_2. The electron is transferred through the Rieske 2Fe-2S cluster and cytochrome c_1 to cyt c. The other electron is used to recycle QH_2 to maximize the efficiency of proton translocation. First, the second electron is taken up by cytochrome b and forwarded to an oxidized coenzyme Q resulting in a semiquinone radical ($Q\bullet^-$). Following, the uptake of a second electron from another QH_2 and two protons from the mitochondrial matrix generate QH_2. The protons from each coenzyme Q are released to the intermembrane space, while the oxidized coenzyme Q diffuses to the Q pool. Thus, two protons are transferred and one cyt c is reduced per QH_2 binding to complex III. Taking recycling of QH_2 into account, three protons are transferred and 1.5 cyt c are reduced per QH_2 generated at complex I and II [60, 66].

6.2.7.4 Cytochrome c-oxidase

The fourth complex oxidizes cyt c through the reduction of oxygen to water. Therefore, not only are protons directly transferred from the mitochondrial matrix to the intermembrane space, but additionally the amount of protons in the matrix is decreased.

Four electrons and thus four cyt c are required for the reduction of one oxygen molecule. Two electrons pass one by one through Cu_A/Cu_B, heme a and heme a_3 to Cu_B, with every other one stopping at heme a_3. The first two electrons build a peroxide bond with one oxygen molecule in between the active centers a_3 and Cu_B. After migration of the third and the fourth electron to Cu_B and a_3, respectively, two protons enter the complex and each attaches to one oxygen molecule splitting the peroxide bond. The resulting hydroxid groups are converted to water by adding an additional proton from the matrix to each oxygen atom, while oxidizing the active center. Water is

released from the complex. During these reactions, four protons are transferred. In summary, on average one cyt c causes the transfer and additionally the uptake of one proton from the mitochondrial matrix [60].

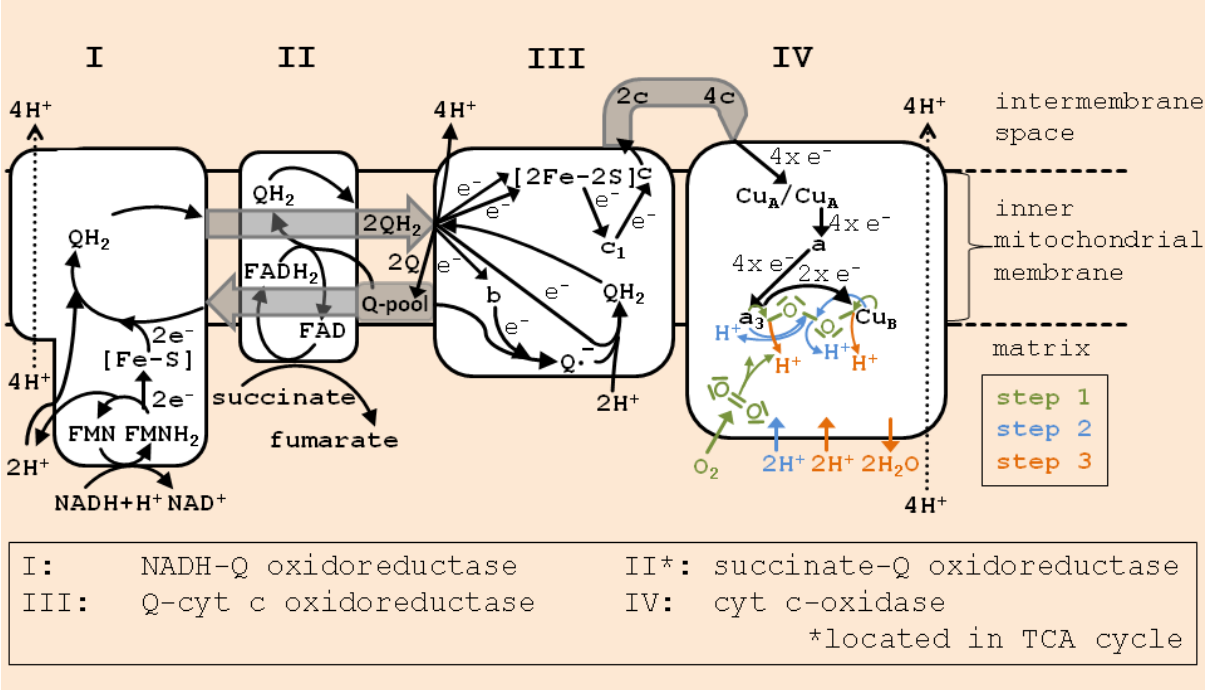

Figure 12: Oxidative phosphorylation. The four complexes of the respiratory chain including their simplified metabolite, proton and electron flows are shown. In complex IV, reaction steps of the reduction from oxygen to water are indicated. A list of all abbreviations is given in Table 5. For a more detailed description see 6.2.7.

6.2.7.5 Adenosine triphosphate synthase

The ATP synthase uses the proton motive force of the proton gradient over the inner mitochondrial membrane to generate chemical energy in the form of ATP. The integral membrane protein complex includes two large subunits F_0 and F_1, each of which consist of several smaller subunits [60]. Among others, the F_0 subunit comprises 10–15 integral membrane proton channels [67]. A proton flux through these channels causes rotation of the proton channels as well as rotation of the stalk. The stalk, built by the γ-subunit of the ATP synthase, belongs to F_1 and connects the integral membrane proteins to the ones in the mitochondrial matrix, namely, the $\alpha_3\beta_3$ hexamer. The β subunits shift their state due to confirmation changes from loose over tight to open every 120°. First, inorganic phosphate and ADP are bound, then the catalysis takes place and finally ATP is released. Thus, a rotation of 360° causes the release of three ATP on average. The number of proton channels determines the number of protons required for an entire rotation [60]. For *Chlamydomonas reinhardtii*, 13 proton channels have been considered based on migration behavior in SDS gels [68]. In conclusion, a yield of three ATP on 13 translocated protons is assumed. Additionally, one proton is required for cotransport of inorganic phosphate to the mitochondrial matrix [59].

6.2.8 Respiration and conversion yields

The metabolic reactions in TAG, starch and other carbohydrate degradations (6.2.4.1 to 6.2.7) are used to estimate net balances of energy carriers (Table 3). These values are estimated to calculate theoretical yields (6.2.1).

The oxidative phosphorylation yields 8.5 and 4.5 protons that are translocated from the matrix to the intermembrane space per NADH and $FADH_2$, respectively. Both NADH and $FADH_2$ also cause the uptake of 1.5 protons for the reaction to water in complex IV. The proton motive force driving ATP synthesis is caused by a gradient in proton concentration and potential [69]. A pH difference of 0.9 units was measured across the inner mitochondrial membrane in human cells [70]. This pH value occurs with an eightfold higher proton concentration in the intermembrane space. For the present calculation the same ratio for the number of protons present in each compartment is assumed. Based on this assumption, approximately 89% of the protons, taken up from the matrix forming water, need to be transferred from the intermembrane space to the matrix to keep the concentration difference constant. The number of transferred protons per proton incorporated into water increases to 96%, assuming a higher pH difference of 1.4 [69]. However, the flow caused by the protons taken up can only be determined precisely by the ratio of the amounts of protons instead of concentrations. In conclusion, NADH and $FADH_2$ cause 9.835 and 5.835 protons to pass from the intermembrane space to the matrix through the ATP synthase, respectively. Yields of ten translocated protons on NADH and six translocated protons on $FADH_2$ are commonly assumed [39].

Textbooks report the synthesis of one ATP is caused by four translocated protons [60]. This occurs with coupling factors from NADH and $FADH_2$ to ATP of 2.5 and 1.5, respectively [39]. Based on the enzyme characteristics described in chapter 6.2.7.5, each ATP requires a flux of 4.333 protons. One additional proton is used for transportation across the inner mitochondrial membrane, resulting in a distinct higher flux of 5.333 protons for one ATP [39, 60]. For other transportation processes no specific energy requirements are taken into account.

Linking the ratios of translocated protons and ATP synthesis gives 1.844 ATP/NADH and 1.094 ATP/$FADH_2$. Based on these values, yields of ATP on different biomass constituents are estimated. NADH and NADPH as well as ATP and GTP are handled as equivalents.

One glucose molecule results in 10 NADH, 2 $FADH_2$ and 4 ATP, thus, 24.628 ATP equivalents, if passing through glycolysis. One eighth is expected to be degraded through OPPP. This pathway gives 12 NADPH and costs 1 ATP, so just 21.128 ATP equivalents as a net balance. Since glucose exists as dehydrated polymers, a molecular weight of 162.14 g/mol needs to be considered per unit. Taking

both pathways into account, the average yield of ATP on starch and other carbohydrates is 0.149 mol ATP/g starch or other sugar polymers.

The yield of ATP on TAG is calculated using an analogous approach. One TAG, consisting of one glycerin and three fatty acids (C18), gains 111 NADH, 52 $FADH_2$ and 26 ATP as a net balance. One TAG molecule with a molecular weight of 885.43 g/mol results in 287.572 ATP equivalents. This gives the average TAG yield 0.325 mol ATP/g TAG.

6.3 Lists of abbreviations, symbols and supplementary materials

Table 4: Abbreviations and symbols. For reaction rates (r_i) and yields (yi) see Table 2 (p. 31)

Abbreviation	Definition
a	absorption cross section (Eq. 23)
a_{rep}	absorption cross section under nitrogen replete conditions (continuous), maximum absorption cross section (day night cycles)
ATP	adenosine triphosphate
C.l.	*Chlorococcum littorale*
cCHO	carbohydrate other than starch fraction as a function of cultivation time
cd	total cultivation duration
CHO (CHO_0)	(initial) concentration of carbohydrates other than starch excluding carbohydrates in reproducing biomass
cont	continuous light
c_x (cx_0)	(initial) biomass concentration
dds	duration of one day
degSTA	concentration of degraded starch from reproducing biomass $\mathrm{degSTA} = \overline{c_x} \cdot \overline{\mathrm{STAinXdeg}} \cdot \Delta t$, with Δt: time range of insufficient light supply for maintenance and means of all values during this period $\mathrm{degSTA} = \mathrm{degSTA} + c_x \cdot \mathrm{STAinXdeg} \cdot \Delta t$, for each time step of sufficient light supply as long as degSTA<0
dlds	duration of light per day
dn	day night cycles
DW	dry weight
f_{part}	partition coefficient for replacing starch in reproducing biomass (Eq. 12)
f_{TAG}	partition coefficient for STA and TAG synthesis under nitrogen deplete conditions
I_0	incident light intensity
m_s	maintenance requirement per amount of reproducing biomass and time
N (N_0)	(initial) concentration of nitrogen in
nd	integer of completed cultivation days (t/dds adjusted downward)
pA, pB	coefficients for photon partitioning in $f_{TAG} = pA \cdot Q^{-pB}$, for details on estimation see supplementary material S 3
Q	cellular nitrogen content
qCHO	biomass specific production rate of carbohydrates other than starch
Q_{deg}	nitrogen content below starch is converted to TAG
Q_{max}	maximum cellular nitrogen content (continuous), nitrogen content at maximum absorption cross section (day night cycles)
Q_{min}	lowest nitrogen content achieved under applied conditions
qN	biomass specific consumption rate of dissolved nitrogen
$q_{ph,avg}$	average biomass specific photosynthetic rate throughout the reactor (Eq. 21)
$q_{ph,max}$	maximum biomass specific photosynthetic rate during nitrogen starvation (Eq. 20)
$q_{ph,max,rep}$	maximum biomass specific photosynthetic rate at nitrogen replete conditions, $q_{ph,max,rep} = \frac{\mu_{max}}{yXph} = \frac{\ln(cx_{t2} - cx_{t1})}{(t_2 - t_1) \cdot yXph}$
qSTA	biomass specific production rate of starch
qTAG	biomass specific production rate of triacylglycerides
qX	biomass specific production rate of reproducing biomass
QY	photosynthetic quantum yield (continuous light: (Eq. 24), day night cycles: (Eq. 5))
S.o	*Scenedesmus obliquus*
STA (STA_0)	(initial) concentration of starch excluding starch in reproducing biomass
STAinXdeg	degradation rate of starch from reproducing biomass
t	cultivation time
TAG (TAG_0)	(initial) concentration of triacylglycerides
X (X_0)	(initial) concentration of reproducing biomass
XCHO	carbohydrate other than starch fraction in biomass after nitrogen depletion
XCHOX	carbohydrate other than starch fraction in reproducing biomass
XSTAX	starch fraction in reproducing biomass
z	light path of the reactor

Table 5: List of abbreviations from chapter 6.2.4.

abbreviation	definition
1,3-BPG	1,3-bisphosphoglycerate
3-PGA	3-phosphoglycerate
6-PG	6-phosphogluconate
6-PGL	6-phosphoglucolactone
ADP	adenosine diphosphate
AMP	adenosine monophosphate
ATP	adenosine triphosphate
CoA	coenzyme A
cyt c / c	cytochrome c
FA	fatty acids
$FADH_2$ / FAD	flavin adenine dinucleotide
FMN	flavin mononucleotide
Fru-1,6P2	fructose 1,6-bisphosphate
Fru-6-P	fructose-6-phosphate
G3P	glyceraldehyde-3-phosphate
G6P	glucose 6-phosphate
GDP	guanosine diphosphate
GTP	guanosine triphosphate
NADH / NAD^+	nicotinamide adenine dinucleotide
NADPH / $NADP^+$	nicotinamide adenine dinucleotide phosphate
OPPP	oxidative pentose-phosphate pathway
PEP	phosphoenolpyruvat
$Q\bullet^-$	semiquinone radical
QH_2	reduced coenzyme Q, ubiquinol
R5P	ribose-5-phosphate
Ru5P	ribulose-5-phosphate
TAG(s)	triacylglycerides(s)
TCA	tricarboxylic acid

Table 6: Supplementary material.

no.	filename
S 1	matlab files model continuous light.zip
S 2	matlab files model day night cycles.zip
S 3	data evaluation and parameter estimation.xlsx
S 4	estimation of maintenance requirement.xlsx
S 5	estimation of fpart.xlsx
S 6	local sensitivity analysis continuous light.xlsx
S 7	local sensitivity analysis day night cycles.xlsx
S 8	measurements of each time point continuous light.xlsx
S 9	measurements of each time point day night cycles.xlsx
S 10	absorption cross section of each time point continuous light.xlsx
S 11	absorption cross section of each time point day night cycles.xlsx
S 12	starch analysis.xlsx
S 13	total carbohydrate analysis.xlsx
S 14	triacylglyceride analysis.xlsx

7 References

1. REN21, *Renewables 2013 Global Status Report.* Paris: REN21 Secretariat., 2013.
2. REN21, *Renewables 2014 Global Status Report.* Paris: REN21 Secretariat., 2014.
3. Wijffels, R.H. and M.J. Barbosa, *An outlook on microalgal biofuels.* Science(Washington), 2010. **329**(5993): p. 796-799.
4. Ho, D.P., H.H. Ngo, and W. Guo, *A mini review on renewable sources for biofuel.* Bioresource Technology, 2014. **169**(0): p. 742-749.
5. IEA, *World Energy Outlook 2012.* International Energy Agency. IEA/OECD, Paris., 2012.
6. Abdelaziz, A.E., G.B. Leite, and P.C. Hallenbeck, *Addressing the challenges for sustainable production of algal biofuels: II. Harvesting and conversion to biofuels.* Environmental technology, 2013. **34**(13-14): p. 1807-1836.
7. Ozkan, A., et al., *Reduction of water and energy requirement of algae cultivation using an algae biofilm photobioreactor.* Bioresource Technology, 2012. **114**: p. 542-548.
8. Waltz, E., *Biotech's green gold?* Nature biotechnology, 2009. **27**(1): p. 15-18.
9. Lardon, L., et al., *Life-cycle assessment of biodiesel production from microalgae.* Environmental science & technology, 2009. **43**(17): p. 6475-6481.
10. Slade, R. and A. Bauen, *Micro-algae cultivation for biofuels: cost, energy balance, environmental impacts and future prospects.* Biomass and Bioenergy, 2013. **53**: p. 29-38.
11. Gouveia, L., *From Tiny Microalgae to Huge Biorefineries.* Oceanography, 2014. **2**(120): p. 2.
12. Pulz, O. and W. Gross, *Valuable products from biotechnology of microalgae.* Applied microbiology and biotechnology, 2004. **65**(6): p. 635-648.
13. Janssen, P.J., et al., *PHOTOSYNTHESIS AT THE FOREFRONT OF A SUSTAINABLE LIFE.* Agricultural Biological Chemistry, 2014. **2**: p. 36.
14. Slegers, P.M., et al., *Design scenarios for flat panel photobioreactors.* Applied Energy, 2011. **88**(10): p. 3342-3353.
15. Bernard, O. and B. Rémond, *Validation of a simple model accounting for light and temperature effect on microalgal growth.* Bioresource technology, 2012. **123**: p. 520-527.
16. Bernard, O., *Hurdles and challenges for modelling and control of microalgae for CO 2 mitigation and biofuel production.* Journal of Process Control, 2011. **21**(10): p. 1378-1389.
17. Wijffels, R., M. Barbosa, and M. Eppink, *Microalgae for the production of bulk chemicals and biofuels.* Biofuels Bioprod Biorefin, 2010. **4**(3): p. 287 - 295.
18. Slegers, P.M., et al., *Scenario analysis of large scale algae production in tubular photobioreactors.* Applied Energy, 2013. **105**(0): p. 395-406.
19. Slegers, P., et al., *Scenario evaluation of open pond microalgae production.* Algal Research, 2013. **2**(4): p. 358-368.
20. Geider, R.J., H.L. MacIntyre, and T.M. Kana, *A Dynamic Regulatory Model of Phytoplanktonic Acclimation to Light, Nutrients, and Temperature.* Limnology and Oceanography, 1998. **43**(4): p. 679-694.
21. Lee, E., et al., *Design tool and guidelines for outdoor photobioreactors.* Chemical Engineering Science, 2014. **106**: p. 18-29.
22. Dillschneider, R. and C. Posten, *A linear programming approach for modeling and simulation of growth and lipid accumulation of phaeodactylum tricornutum.* Energies, 2013. **6**(10): p. 5333-5356.
23. Kliphuis, A.M., et al., *Metabolic modeling of Chlamydomonas reinhardtii: energy requirements for photoautotrophic growth and maintenance.* Journal of applied phycology, 2012. **24**(2): p. 253-266.
24. Klok, A.J., et al., *A model for customising biomass composition in continuous microalgae production.* Bioresource Technology, 2013. **146**: p. 89-100.
25. Packer, A., et al., *Growth and neutral lipid synthesis in green microalgae: A mathematical model.* Bioresource Technology, 2011. **102**(1): p. 111-117.
26. Mairet, F., et al., *Modelling neutral lipid production by the microalga Isochrysis aff. galbana under nitrogen limitation.* Bioresource Technology, 2011. **102**(1): p. 142-149.

27. Breuer, G., et al., *Improving areal TAG productivity of microalgae - A model based approach.* (unpublished work), 2014.
28. Breuer, G., et al., *The impact of nitrogen starvation on the dynamics of triacylglycerol accumulation in nine microalgae strains.* Bioresource Technology, 2012. **124**(0): p. 217-226.
29. Griffiths, M.J., R.P. Hille, and S.T.L. Harrison, *Lipid productivity, settling potential and fatty acid profile of 11 microalgal species grown under nitrogen replete and limited conditions.* Journal of Applied Phycology, 2011.
30. Liu, J., F. Chen, and J. Huang, *Microalgae as feedstocks for biodiesel production*. 2011: INTECH Open Access Publisher.
31. Ota, M., et al., *Fatty acid production from a highly CO 2 tolerant alga, Chlorocuccum littorale, in the presence of inorganic carbon and nitrate.* Bioresource Technology, 2009. **100**(21): p. 5237-5242.
32. Berberoglu, H., P.S. Gomez, and L. Pilon, *Radiation characteristics of Botryococcus braunii, Chlorococcum littorale, and Chlorella sp. used for fixation and biofuel production.* Journal of Quantitative Spectroscopy and Radiative Transfer, 2009. **110**(17): p. 1879-1893.
33. Hu, Q., et al., *Ultrahigh-cell-density culture of a marine green alga Chlorococcum littorale in a flat-plate photobioreactor.* Applied Microbiology and Biotechnology, 1998. **49**(6): p. 655-662.
34. Breuer, G., et al., *The impact of nitrogen starvation on the dynamics of triacylglycerol accumulation in nine microalgae strains.* Bioresour Technol, 2012. **124**: p. 217 - 226.
35. Dubois, M., et al., *Colorimetric method for determination of sugars and related substances.* Analytical chemistry, 1956. **28**(3): p. 350-356.
36. Chen, C.-Y., et al., *Microalgae-based carbohydrates for biofuel production.* Biochemical Engineering Journal, 2013. **78**: p. 1-10.
37. Jakob, T., et al., *A complete energy balance from photons to new biomass reveals a light-and nutrient-dependent variability in the metabolic costs of carbon assimilation.* Journal of experimental botany, 2007. **58**(8): p. 2101-2112.
38. Torzillo, G., A. Sacchi, and R. Materassi, *Temperature as an important factor affecting productivity and night biomass loss in Spirulina platensis grown outdoors in tubular photobioreactors.* Bioresource technology, 1991. **38**(2): p. 95-100.
39. Johnson, X. and J. Alric, *Central carbon metabolism and electron transport in Chlamydomonas reinhardtii: metabolic constraints for carbon partitioning between oil and starch.* Eukaryotic cell, 2013. **12**(6): p. 776-793.
40. Han, F., et al., *Changes of biomass, lipid content and fatty acids composition under a light–dark cyclic culture of Chlorella pyrenoidosa in response to different temperature.* Bioresource Technology, 2013. **132**(0): p. 182-189.
41. Benvenuti, G., et al., *Selecting microalgae with high lipid productivity and photosynthetic activity under nitrogen starvation.* Journal of Applied Phycology, 2014: p. 1-7.
42. Breuer, G., et al., *Superior triacylglycerol (TAG) accumulation in starchless mutants of Scenedesmus obliquus:(II) evaluation of TAG yield and productivity in controlled photobioreactors.* Biotechnology for biofuels, 2014. **7**(1): p. 1-11.
43. Chisti, Y., *Biodiesel from microalgae.* Biotechnology Advances, 2007. **25**(3): p. 294-306.
44. Grobbelaar, J.U. and C.J. Soeder, *Respiration losses in planktonic green algae cultivated in raceway ponds.* Journal of plankton research, 1985. **7**(4): p. 497-506.
45. Reddy, S., *University Botany I:(Algae, Fungi, Bryophyta And Pteridophyta)*. Vol. 1. 2001: New Age International.
46. Geider, R.J., H.L. MacIntyre, and T.M. Kana, *A dynamic regulatory model of phytoplanktonic acclimation to light, nutrients, and temperature.* Limnology and Oceanography, 1998. **43**(4): p. 679-694.
47. Cuhel, R.L., P.B. Ortner, and D.R. Lean, *Night synthesis of protein by algae1.* Limnology and Oceanography, 1984. **29**(4): p. 731-744.
48. Hu, Q., et al., *Microalgal triacylglycerols as feedstocks for biofuel production: perspectives and advances.* Plant J, 2008. **54**(4): p. 621 - 639.

49. Sharma, K.K., H. Schuhmann, and P.M. Schenk, *High lipid induction in microalgae for biodiesel production.* Energies, 2012. **5**(5): p. 1532-1553.
50. Buléon, A., et al., *Starch granules: structure and biosynthesis.* International Journal of Biological Macromolecules, 1998. **23**(2): p. 85-112.
51. Kruger, N.J. and A. von Schaewen, *The oxidative pentose phosphate pathway: structure and organisation.* Current Opinion in Plant Biology, 2003. **6**(3): p. 236-246.
52. Sweetlove, L.J. and A.R. Fernie, *Regulation of metabolic networks: understanding metabolic complexity in the systems biology era.* New Phytologist, 2005. **168**(1): p. 9-24.
53. Blum, P., *Archaea: new models for prokaryotic biology*. 2008: Horizon Scientific Press.
54. Plaxton, W.C., *THE ORGANIZATION AND REGULATION OF PLANT GLYCOLYSIS.* Annual Review of Plant Physiology and Plant Molecular Biology, 1996. **47**(1): p. 185-214.
55. Koolman, J., *Taschenatlas der Biochemie*. 2003: Georg Thieme Verlag.
56. Tsujimoto, Y., T. Nakagawa, and S. Shimizu, *Mitochondrial membrane permeability transition and cell death.* Biochimica et Biophysica Acta (BBA) - Bioenergetics, 2006. **1757**(9–10): p. 1297-1300.
57. Herzig, S., et al., *Identification and Functional Expression of the Mitochondrial Pyruvate Carrier.* Science, 2012. **337**(6090): p. 93-96.
58. Korkes, S., et al., *Enzymatic synthesis of citric acid IV. Pyruvate as acetyl donor.* Journal of Biological Chemistry, 1951. **193**(2): p. 721-735.
59. Kreutzig, T., *Kurzlehrbuch Biochemie* 2006: Elsevier, Urban&FischerVerlag.
60. Berg, J., J. Tymoczoko, and L. Stryer, *Biochemie, 6th edition, 2007*. Elsevier GmbH, München.
61. natureEDUCATION, *Reactions of β-oxidation.* 2010.
62. Cabanelas, I.T.D., et al., *Rapid method to screen and sort lipid accumulating microalgae.* Bioresource Technology, (0).
63. natureEDUCATION, *Reactions of tricarboxylic acid cycle.* 2010.
64. Ying, W., *NAD+/NADH and NADP+/NADPH in cellular functions and cell death: regulation and biological consequences.* Antioxidants & redox signaling, 2008. **10**(2): p. 179-206.
65. Kikkawa, S., et al., *Conversion of GDP into GTP by nucleoside diphosphate kinase on the GTP-binding proteins.* Journal of Biological Chemistry, 1990. **265**(35): p. 21536-21540.
66. Enriquez, J.A. and G. Lenaz, *Coenzyme Q and the Respiratory Chain: Coenzyme Q Pool and Mitochondrial Supercomplexes.* Molecular syndromology, 2014. **5**(3-4): p. 119.
67. Kucharczyk, R., et al., *Mitochondrial ATP synthase disorders: Molecular mechanisms and the quest for curative therapeutic approaches.* Biochimica et Biophysica Acta (BBA) - Molecular Cell Research, 2009. **1793**(1): p. 186-199.
68. Meyer zu Tittingdorf, J.M.W., et al., *The stoichiometry of the chloroplast ATP synthase oligomer III in Chlamydomonas reinhardtii is not affected by the metabolic state.* Biochimica et Biophysica Acta (BBA) - Bioenergetics, 2004. **1659**(1): p. 92-99.
69. Berg, J.M., J.L. Tymoczko, and L. Stryer, *A Proton Gradient Powers the Synthesis of ATP.* 2002.
70. Porcelli, A.M., et al., *pH difference across the outer mitochondrial membrane measured with a green fluorescent protein mutant.* Biochemical and Biophysical Research Communications, 2005. **326**(4): p. 799-804.